JCTC Journal of Chemical Theory and Computation

pubs.acs.org/JCTC Article

Active Spaces and Non-Orthogonal Configuration Interaction Approaches for Investigating Molecules on Metal Surfaces

Junhan Chen, Wenjie Dou, and Joseph Subotnik*

Cite This: https://doi.org/10.1021/acs.jctc.2c00740 Read Online

ACCESS | Metrics & More | Article Recommendations

ABSTRACT: We test a set of multiconfigurational wavefunction approaches for calculating the ground state electron population for a two-site Anderson model representing a molecule on a metal surface. In particular, we compare (i) a Hartree Fock like wavefunction where frontier orbitals are allowed to be nonorthogonal versus (ii) a fully non-orthogonal configuration interaction wavefunction based on constrained Hartree−Fock states. We test both the strong and weak metal-molecule hybridization (Γ) limits as well as the strong and weak electron−electron repulsion (U) limits. We obtain accurate results as compared with exact numerical renormalization group theory, recovering charge transfer states where appropriate. The current framework should open a path to run molecular non-adiabatic dynamics on metal surfaces.

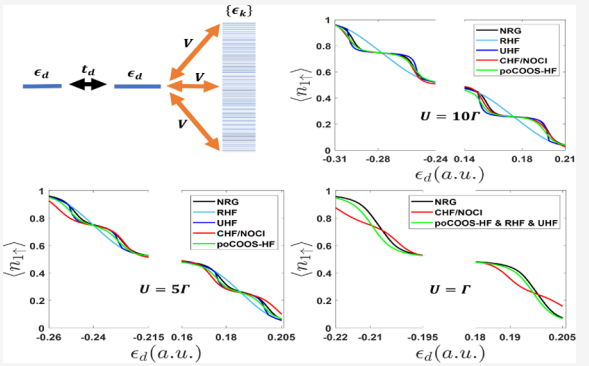

1. INTRODUCTION

Solving embedding problem has attracted a great deal of attention in recent years[1−11] as chemists explore interesting interfacial phenomena, for example, molecular resonance effects on metal surfaces,[12] electron-coupled adsorption[13] and electron-coupled vibrations.[14,15] Embedding theory provides an attractive strategy to describe the electronic structure of extended systems (including interfacial systems) which can be impractical for traditional high accuracy quantum mechanics methods, for example coupled-cluster singles, doubles and full triples,[16] second-order perturbation with complete active space (CASPT2)[17,18] and multireference configuration interaction[19] or full configuration interaction.[20,21]

Historically, some of the earliest embedding calculations have addressed the Anderson Impurity model[22] (or the more general Hubbard model). By now, this model has been analyzed by a variety of exact impurity solvers including the numerical renormalization group (NRG),[23] exact diagonalization[24] and quantum monte carlo.[25] These benchmark studies have then been very useful as far as benchmarking other, not exact but powerful, embedding methods, including dynamical mean-field theory[26] and density matrix embedding theory.[5] To date, however, many of these powerful methods still have not been applied to study the problem of embedding realistic molecules on a realistic metal surface where there are many two-electron matrix elements. For such a mundane task, constrained DFT (CDFT) still remains the most practical approach, and the method has been applied successfully to some extent.[27−30] That being said, CDFT results can also be unreliable in some cases, for example strong molecule-metal coupling (i.e. strong hybridization)[12] and fractional charge transfer.[31] Nonadiabatic dynamics remains just out of reach for many realistic potentials.

With this background in mind, the goal of this paper is to introduce an new electronic structure method designed specifically to address a molecule on a metal surface. Importantly, when the electron−electron repulsion energy on the impurity becomes large compared with the impurity-metal coupling (i.e. in the weak metal-molecule coupling limit), the true wavefunction will exhibit strong multireference character. In such a case, we must be able to capture the open-shell singlet character for an electron on or off the impurity; a single determinant wavefunction will not be a good reference in such a case. At the same time, of course, the correct wavefunction will exhibit simple single-reference character in the limit of strong metal-molecule coupling, and a good solver must reduce to the RHF solution in such a case. With these two limits in mind, below we explore a very basic approach whereby the frontier orbitals are modulated so that the total wavefunction will indeed contain open-shell character in the weak coupling limit and closed-shell character in the strong coupling limit. We call the resulting ansatz a closed-or-open shell Hartree Fock (COOS-HF) wavefunction.

Received: July 18, 2022

In what follows, our specific goal will be to derive the necessary equations for solving for the COOS-HF equations just described, to apply this method to the Anderson Impurity model, and to compare our results to a constrained Hartree−Fock/Nonorthogonal configuration interaction (CHF/NOCI) formalism. We will show that surprisingly accurate results can be found with only a few variables to be optimized. We note that these results follow our previous work in embedding using configuration interaction spaces,[32,33] but we emphasize that the present approach does not require diagonalizing a massive matrix of any kind.

An outline of this manuscript is as follows. In Section 2, we introduce the COOS-HF formalism and we review the basic elements of a standard CHF/NOCI approach; we also include a brief comparison between COOS-HF and CASSCF(2,2) in Section 2.3.1. In Section 3, we show results for the ground state population and energy, from which one can evaluate the accuracy of our approach. In Section 4, we discuss spin-contamination and show that the present approach is free of any contamination. Furthermore, we contemplate different variations of the COOS-HF ansatz that one can imagine implementing [e.g., (partially optimized) poCOOS-HF vs (fully optimized) foCOOS-HF] and we place our results in the context of a CASSCF(2,2) formalism. We conclude in Section 5.

2. THEORY

2.1. Model: Two-Site Anderson Impurity Model. For this paper, our model of choice will be the two-site Anderson impurity model (AIM). Within a second quantized representation, the Hamiltonian can be written as

$$\begin{aligned}\hat{H} &= \hat{H}_{\text{one}} + \hat{\Pi}\\ \hat{H}_{\text{one}} &= \epsilon_{d_1}\sum_{\sigma} d_{1\sigma}^{\dagger}d_{1\sigma} + \epsilon_{d_2}\sum_{\sigma} d_{2\sigma}^{\dagger}d_{2\sigma}\\ &\quad + t_d\sum_{\sigma}(d_{1\sigma}^{\dagger}d_{2\sigma} + d_{2\sigma}^{\dagger}d_{1\sigma})\\ &\quad + \sum_{k\sigma}\epsilon_{k\sigma}c_{k\sigma}^{\dagger}c_{k\sigma} + \sum_{k\sigma}V_k(d_{1\sigma}^{\dagger}c_{k\sigma} + c_{k\sigma}^{\dagger}d_{1\sigma})\\ \hat{\Pi} &= U(d_{1\uparrow}^{\dagger}d_{1\uparrow}d_{1\downarrow}^{\dagger}d_{1\downarrow} + d_{2\uparrow}^{\dagger}d_{2\uparrow}d_{2\downarrow}^{\dagger}d_{2\downarrow})\end{aligned} \tag{1}$$

and the mean-field Fock operator (assuming the spin restricted case) can be easily written as

$$\hat{F} = \hat{H}_{\text{one}} + U\langle d_1^{\dagger}d_1\rangle d_1^{\dagger}d_1 + U\langle d_2^{\dagger}d_2\rangle d_2^{\dagger}d_2 \tag{2}$$

Here, $\{\widehat{d_1}^{\dagger}, \widehat{d_2}^{\dagger}\}$ refer to impurity atomic orbitals, the operators $\{\widehat{c_k}^{\dagger}\}$ refer to bath (metal surface) atomic orbitals, and σ refers to an electron spin. ϵ_{d_1}, ϵ_{d_2} and ϵ_k are one-electron ionization energies for the impurities and bath. t_d is the hopping parameter between site 1 and site 2, U represents the on-site coulomb repulsion for the impurity. V_k represents the hybridization between impurity site 1 and the metal bath, and as in the wide band approximation, is characterized by

$$\Gamma = \Gamma(\epsilon) = 2\pi\sum_k |V_k|^2\,\delta(\epsilon - \epsilon_k) \tag{3}$$

where Γ is assumed to be constant through the whole energy spectrum ϵ.

The Hamiltonian in eq 1 characterizes many different physical processes because, in certain parameter regimes, one can identify states with effectively open shell singlet character within the set of impurity orbitals; in other regimes, one can identify charge transfer between impurity and metal; and of course these two phenomena cannot be fully disentangled for all parameter regimes, highlighting a more realistic version of electron−electron correlation than is found for a single-site Anderson Holstein Hamiltonian. Note that the two-site model in this paper assumes that two impurity sites have the same energy, that is $\epsilon_{d1} = \epsilon_{d2} = \epsilon_d$, but we believe our results here are general. For a schematic figure of the physical set up, see Figure 1.

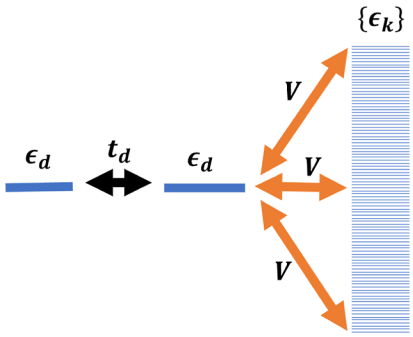

Figure 1. Schematic figure for a two-site model with 800 non-interaction bath states.

We will now address the two wavefunction approaches that we wish to compare as far as assessing the ground-state electronic structure for the system plus bath: a constrained Hartree Fock configuration interaction approach versus a closed-or-open-shell frontier orbital wavefunction approach.

2.2. Method 1: Constrained Hartree−Fock Based Nonorthogonal Configuration Interaction. *2.2.1. Constrained HF States.* Following ref 34, a general constraint to the density can often be written as

$$\sum_{\sigma}\int w_c^{\sigma}(\boldsymbol{r})\rho^{\sigma}(\boldsymbol{r})\mathrm{d}\boldsymbol{r} = N_c \tag{4}$$

where $w_c(\boldsymbol{r})$ acts as a weight function that defines the constrained property, σ represents the electron spin, $\rho(\boldsymbol{r})$ represents the charge density and N_c represents the total number of constrained charge (or electrons). By adding one Lagrange multiplier, V_c, one can optimize a general functional of the density $E[\rho]$ with a prescribed constraint by looking for extrema of the following function

$$W[\rho, V_c] = E[\rho] + V_c\left(\sum_{\sigma}\int w_c^{\sigma}(\boldsymbol{r})\rho^{\sigma}(\boldsymbol{r})\mathrm{d}\boldsymbol{r} - N_c\right) \tag{5}$$

Within constrained density functional theory,[34] one looks to minimize the energy functional with the constraint that orbitals are normalized, and one then arrives as the standard constrained DFT equations

$$\left(-\frac{1}{2}\nabla^2 + v_n(\boldsymbol{r}) + \int\frac{\rho(\boldsymbol{r}')}{|\boldsymbol{r}-\boldsymbol{r}'|}\mathrm{d}\boldsymbol{r}' + v_{xc\sigma}(\boldsymbol{r}) + V_c w_c^{\sigma}(\boldsymbol{r})\right)\psi_{i\sigma} = \epsilon_{i\sigma}\psi_{i\sigma} \tag{6}$$

This language (based on continuous real space or plane wave basis sets) can easily be extended to the realm of discretized site basis sets as appropriate for a generalized Anderson model under a restricted Hartree−Fock (RHF) framework. The relevant

https://doi.org/10.1021/acs.jctc.2c00740
J. Chem. Theory Comput. XXXX, XXX, XXX−XXX

density constraint (defining the number of electrons on the impurity) becomes

$$\mathrm{Tr}(\hat{\rho}\hat{w}_c) = N_c \tag{7}$$

where the density matrix $\hat{\rho}$ and the weight matrix $\hat{w_c}$ are defined as:

$$\hat{\rho} = \sum_{i\in\mathrm{occ}} |\psi_i\rangle\langle\psi_i| \tag{8}$$

$$\hat{w}_c = \sum_{\mu\in\mathrm{impurity}} w_\mu |d_\mu\rangle\langle d_\mu| \tag{9}$$

Here, the set $\{|\psi_i\rangle\}$ are the eigenvectors of the Hartree−Fock equation and we set all site weights as $w_\mu = 1$. Specifically speaking, the weight matrix for two-site Anderson model will be

$$\hat{w}_c = |d_1\rangle\langle d_1| + |d_2\rangle\langle d_2| \tag{10}$$

We will explore all possible integer values for the constrained number of integer electrons on the two impurity sites:

$$N_c \in \{0e, 1e, 2e, 3e, 4e\} \tag{11}$$

The final constrained Hartree−Fock equation (like the constrained DFT equations in eq 6) can be written as

$$(\hat{F} + V_c\hat{w}_c)\psi_i = \epsilon_i\psi_i \tag{12}$$

where the fock matrix $\hat{F}$ is defined in eq 2. Note that even though N_c is not explicitly included in eq 12, a value of N_c is required to find the optimized Lagrange multiplier, V_c, which satisfies $\frac{dW}{dV_c} = 0$.

To calculate V_c, we use the first and second derivatives[34] of $W(V_c)$ (assuming restricted orbitals) in eq 5

$$\begin{aligned}\frac{\mathrm{d}W}{\mathrm{d}V_c} &= \sum_\sigma \int w_c^\sigma(\boldsymbol{r})\rho^\sigma(\boldsymbol{r})d\boldsymbol{r} - N_c \\ &= 2\langle d_1|\hat{\rho}|d_1\rangle + 2\langle d_2|\hat{\rho}|d_2\rangle - N_c\end{aligned} \tag{13}$$

$$\begin{aligned}\frac{\mathrm{d}^2W}{\mathrm{d}V_c^2} &= 2\sum_\sigma \sum_i^{N_\sigma} \sum_{a>N_\sigma} \frac{|\langle\psi_{i\sigma}|w_c^\sigma|\psi_{a\sigma}\rangle|^2}{\epsilon_{i\sigma} - \epsilon_{a\sigma}} \\ &= 4\sum_{i\in\mathrm{occ}} \sum_{a\in\mathrm{vir}} \frac{|\langle\psi_i|w_c|\psi_a\rangle|^2}{\epsilon_i - \epsilon_a}\end{aligned} \tag{14}$$

Here $\hat{\rho}$ is the density matrix operator defined in eq 8, d_1 and d_2 represent two impurity sites, w_c is the weight matrix defined in eq 10, $\{\psi_i\}$ or $\{\psi_a\}$ and ϵ_i or ϵ_a are eigenvectors and eigenvalues of eq 12, respectively. As discussed in ref 34, eq 14 is derived from simple first-order perturbation theory of the Kohn−Sham equations. An algorithm to determine the constrained Hartree−Fock solution can be summarised as follows

1 Choose the desired value of N_c in eq 11
2 Guess a Lagrange multiplier, for example $V_c = 0$
3 Guess an impurity population $\langle d_1^\dagger d_1\rangle = \langle d_2^\dagger d_2\rangle = \frac{N_c}{4}$
4 Construct the Fock matrix using eq 2
5 Solve eq 12 self-consistently and obtain eigenvectors $\{\psi\}$ and eigenvalues $\{\epsilon\}$
6 Calculate a new impurity population $\langle d_1^\dagger d_1\rangle$ and $\langle d_2^\dagger d_2\rangle$
7 Use eqs 13 and 14, take a Newton step toward a stationary solution for W and calculate a new V_c.
8 Repeat Steps 4−7 until V_c converges.

2.2.2. Non-orthogonal Configuration Interaction. The total number of electrons on the two impurity sites is required to be an integer between 0 and 4. Therefore, one naturally finds five diabatic constrained Hartree−Fock (CHF) states for our model problem: $|\Phi_{4e}\rangle$, $|\Phi_{3e}\rangle$, $|\Phi_{2e}\rangle$, $|\Phi_{1e}\rangle$, $|\Phi_{0e}\rangle$, respectively. Since these configurations are not orthogonal to each other, a configuration interaction Hamiltonian can be constructed as (see Appendix A for a detailed derivation of the necessary matrix elements)

$$H^{\mathrm{CHF/NOCI}} = \begin{bmatrix} \langle\Phi_{4e}|H|\Phi_{4e}\rangle & \langle\Phi_{4e}|H|\Phi_{3e}\rangle & \langle\Phi_{4e}|H|\Phi_{2e}\rangle & \langle\Phi_{4e}|H|\Phi_{1e}\rangle & \langle\Phi_{4e}|H|\Phi_{0e}\rangle \\ \langle\Phi_{3e}|H|\Phi_{4e}\rangle & \langle\Phi_{3e}|H|\Phi_{3e}\rangle & \langle\Phi_{3e}|H|\Phi_{2e}\rangle & \langle\Phi_{3e}|H|\Phi_{1e}\rangle & \langle\Phi_{3e}|H|\Phi_{0e}\rangle \\ \langle\Phi_{2e}|H|\Phi_{4e}\rangle & \langle\Phi_{2e}|H|\Phi_{3e}\rangle & \langle\Phi_{2e}|H|\Phi_{2e}\rangle & \langle\Phi_{2e}|H|\Phi_{1e}\rangle & \langle\Phi_{2e}|H|\Phi_{0e}\rangle \\ \langle\Phi_{1e}|H|\Phi_{4e}\rangle & \langle\Phi_{1e}|H|\Phi_{3e}\rangle & \langle\Phi_{1e}|H|\Phi_{2e}\rangle & \langle\Phi_{1e}|H|\Phi_{1e}\rangle & \langle\Phi_{1e}|H|\Phi_{0e}\rangle \\ \langle\Phi_{0e}|H|\Phi_{4e}\rangle & \langle\Phi_{0e}|H|\Phi_{3e}\rangle & \langle\Phi_{0e}|H|\Phi_{2e}\rangle & \langle\Phi_{0e}|H|\Phi_{1e}\rangle & \langle\Phi_{0e}|H|\Phi_{0e}\rangle \end{bmatrix} \tag{15}$$

and the corresponding overlap S is expressed as

$$S = \begin{bmatrix} 1 & \langle\Phi_{4e}|\Phi_{3e}\rangle & \langle\Phi_{4e}|\Phi_{2e}\rangle & \langle\Phi_{4e}|\Phi_{1e}\rangle & \langle\Phi_{4e}|\Phi_{0e}\rangle \\ \langle\Phi_{3e}|\Phi_{4e}\rangle & 1 & \langle\Phi_{3e}|\Phi_{2e}\rangle & \langle\Phi_{3e}|\Phi_{1e}\rangle & \langle\Phi_{3e}|\Phi_{0e}\rangle \\ \langle\Phi_{2e}|\Phi_{4e}\rangle & \langle\Phi_{2e}|\Phi_{3e}\rangle & 1 & \langle\Phi_{2e}|\Phi_{1e}\rangle & \langle\Phi_{2e}|\Phi_{0e}\rangle \\ \langle\Phi_{1e}|\Phi_{4e}\rangle & \langle\Phi_{1e}|\Phi_{3e}\rangle & \langle\Phi_{1e}|\Phi_{2e}\rangle & 1 & \langle\Phi_{1e}|\Phi_{0e}\rangle \\ \langle\Phi_{0e}|\Phi_{4e}\rangle & \langle\Phi_{0e}|\Phi_{3e}\rangle & \langle\Phi_{0e}|\Phi_{2e}\rangle & \langle\Phi_{0e}|\Phi_{1e}\rangle & 1 \end{bmatrix} \tag{16}$$

To transform the interaction Hamiltonian into an orthogonal configuration basis, a transformation matrix X will be introduced, which satisfies

$$X^\dagger S X = I \tag{17}$$

In this paper, X is chosen as: $X = S^{-1/2}$. By diagonalizing the matrix $X^\dagger H^{\mathrm{CHF/NOCI}} X$, one obtains five adiabatic constrained Hartree−Fock nonorthogonal configuration interaction (CHF/NOCI) states.

2.3. Method 2: COOS-HF. Having discussed a standard CHF/NOCI approach to charge transfer, let us now introduce an alternative multiconfigurational approach that is not based on a configuration interaction Hamiltonian but rather on a set of frontier (non-orthogonal) orbitals. Our approach is to consider a wavefunction of the following form

$$|\Phi_{\mathrm{COOS-HF}}\rangle = \frac{1}{\sqrt{N}}(|\Phi_{pq}\rangle + |\Phi_{qp}\rangle) \tag{18}$$

where N is the normalization factor

$$N = 2(1 + \langle p|q\rangle^2) \tag{19}$$

$\boldsymbol{p}$, $\boldsymbol{q}$ are two nonorthogonal orbitals and $|\Phi_{pq}\rangle$, $|\Phi_{qp}\rangle$ are the following two slater determinants for a $2n$-electron system

$$|\Phi_{pq}\rangle = \begin{vmatrix} \psi_1(1) & \overline{\psi_1}(1) & \cdots & p(1) & \overline{q}(1) \\ \psi_1(2) & \overline{\psi_1}(2) & \cdots & p(2) & \overline{q}(2) \\ \vdots & \vdots & \ddots & \vdots & \vdots \\ \psi_1(2n) & \overline{\psi_1}(2n) & \cdots & p(2n) & \overline{q}(2n) \end{vmatrix} \tag{20}$$

https://doi.org/10.1021/acs.jctc.2c00740
J. Chem. Theory Comput. XXXX, XXX, XXX−XXX

$$|\Phi_{qp}\rangle = \begin{vmatrix} \psi_1(1) & \overline{\psi_1}(1) & \cdots & q(1) & \overline{p}(1) \\ \psi_1(2) & \overline{\psi_1}(2) & \cdots & q(2) & \overline{p}(2) \\ \vdots & \vdots & \ddots & \vdots & \vdots \\ \psi_1(2n) & \overline{\psi_1}(2n) & \cdots & q(2n) & \overline{p}(2n) \end{vmatrix} \quad (21)$$

For the moment, we make no stipulations about the character of the orbitals $\boldsymbol{p}$ and $\boldsymbol{q}$; they could be parallel or they could be orthogonal. And so, we refer to the wavefunction in eq 18 as a closed-or-open shell HF ansatz.

Two options are now possible as far optimizing such a COOS-HF wavefunction. First, one could imagine optimizing all of the orbitals, $\{\psi_1, \psi_2, ..., \boldsymbol{p}, \boldsymbol{q}\}$. We will call this approach a fully optimized COOS-HF (foCOOS-HF) ansatz.

The second approach is simpler and is based on a closed shell RHF reference state. In such a case, we can seek three nonorthogonal orbitals $\boldsymbol{o}$, $\boldsymbol{p}$, $\boldsymbol{q}$, so that a simplified partially optimized COOS-HF (poCOOS-HF) wavefunction can be written as

$$|\Phi_{\text{poCOOS-HF}}\rangle = \frac{1}{\sqrt{N}}(|\psi_1\overline{\psi_1}\psi_2\overline{\psi_2}\ldots\hat{o}\hat{\overline{o}}p\overline{q}\rangle + |\psi_1\overline{\psi_1}\psi_2\overline{\psi_2}\ldots\hat{o}\hat{\overline{o}}q\overline{p}\rangle) \quad (22)$$

$$= \frac{1}{\sqrt{N}}(|\Psi_{o\overline{o}}^{p\overline{q}}\rangle + |\Psi_{o\overline{o}}^{q\overline{p}}\rangle) \quad (23)$$

(22)

In eq 22, the choice of orbitals $\boldsymbol{o}$, $\boldsymbol{p}$, and $\boldsymbol{q}$ is critical. For this wavefunction, we insist that orbital $\boldsymbol{o}$ must be an occupied orbital and this orbital ô is removed in the slater determinant in eq 22, as indicated by a hat. However, we make no such assumption about orbitals $\boldsymbol{p}$ and $\boldsymbol{q}$ (our "active" orbitals); even though p and q have been written for convenience in the superscript of the kets $|\Phi_{o\overline{o}}^{p\overline{q}}\rangle$ and $|\Phi_{o\overline{o}}^{q\overline{p}}\rangle$, these orbital $\boldsymbol{p}$ need not be orthogonal to orbital $\boldsymbol{o}$ or orbital $\boldsymbol{q}$. Thus, when we optimize eq 22 for orbitals $\boldsymbol{o}$, $\boldsymbol{p}$, and $\boldsymbol{q}$, we can indeed recover the starting RHF ansatz by picking $\boldsymbol{o} = \boldsymbol{p} = \boldsymbol{q}$.

In particular, we can parameterize the spatial components of $\boldsymbol{o}$, $\boldsymbol{p}$, and $\boldsymbol{q}$ in the basis of RHF canonical occupied orbitals $\{o_i\}$ and virtual orbitals $\{v_a\}$

$$|o\rangle = \sum_i c_i|o_i\rangle$$

$$|p\rangle = d_o|o\rangle + \sum_a d_a|v_a\rangle$$

$$|q\rangle = \tilde{d}_o|o\rangle + \sum_b \tilde{d}_b|v_b\rangle \quad (24)$$

Note that, if we define the core orbitals to be all of those occupied orbitals $\boldsymbol{i}$ orthogonal to orbital $\boldsymbol{o}$, the following identities also hold

$$\langle i|o\rangle = 0 \quad (25)$$

$$\langle i|p\rangle = 0 \quad (26)$$

$$\langle i|q\rangle = 0 \quad (27)$$

The core orbitals $\boldsymbol{i}$ together with orbital $\boldsymbol{o}$ form the RHF occupied space, that is

$$\sum_i |i\rangle\langle i| + |o\rangle\langle o| = \sum_i |o_i\rangle\langle o_i| \quad (28)$$

2.3.1. COOS-HF as a Subset of a CASSCF(2,2) Calculation. The astute reader will notice that the COOS-HF wavefunction ansatz in eq 18 represents a singlet configuration without spin contamination and that the ansatz is clearly a subset of a CASSCF(2,2) ansatz as can be seen by writing nonorthogonal orbitals $\boldsymbol{p}$, $\boldsymbol{q}$ in the orthonormal basis $\boldsymbol{a}$, $\boldsymbol{b}$.

$$|p\rangle = \cos\theta|a\rangle + \sin\theta|b\rangle$$

$$|q\rangle = \cos\eta|a\rangle + \sin\eta|b\rangle \quad (29)$$

Therefore, the wavefunction in eq 18 can be written as (for simplicity, the core orbitals are ignored)

$$\frac{|p\overline{q}\rangle + |q\overline{p}\rangle}{\sqrt{N}} = \frac{1}{\sqrt{N}}\{2\cos\theta\cos\eta|a\overline{a}\rangle + 2\sin\theta\sin\eta|b\overline{b}\rangle + (\cos\theta\sin\eta + \cos\eta\sin\theta)(|a\overline{b}\rangle + |b\overline{a}\rangle)\} \quad (30)$$

This equation is clearly of the CASSCF(2,2) form (where the CI coefficients would normally be written as)

$$\alpha|a\overline{a}\rangle + \beta|b\overline{b}\rangle + \gamma(|a\overline{b}\rangle + |b\overline{a}\rangle) \quad (31)$$

if one makes the substitution

$$\alpha = \frac{2\cos\theta\cos\eta}{\sqrt{N}}$$

$$\beta = \frac{2\sin\theta\sin\eta}{\sqrt{N}}$$

$$\gamma = \frac{(\cos\theta\sin\eta + \cos\eta\sin\theta)}{\sqrt{N}}$$

$$N = 2 \times [1 + (\cos\theta\cos\eta + \sin\theta\sin\eta)^2] \quad (32)$$

A more complete discussion of this correspondence will be given in the Discussion section.

2.3.2. Solving for the poCOOS-HF Orbitals and Energy. Let us now discuss how one can most easily solve for the poCOOS-HF orbitals. For the ansatz in eq 22, the expectation value for the total energy is

$$\langle\Phi_{\text{poCOOS-HF}}|H|\Phi_{\text{poCOOS-HF}}\rangle = \frac{\langle\Psi_{o\overline{o}}^{p\overline{q}}|H|\Psi_{o\overline{o}}^{p\overline{q}}\rangle + \langle\Psi_{o\overline{o}}^{p\overline{q}}|H|\Psi_{o\overline{o}}^{q\overline{p}}\rangle}{1 + \langle p|q\rangle^2} \quad (33)$$

where

$$\langle\Psi_{o\overline{o}}^{p\overline{q}}|H|\Psi_{o\overline{o}}^{p\overline{q}}\rangle = \langle\ldots i\ldots p\ldots \overline{i}\ldots\overline{q}|H|\ldots i\ldots p\ldots\overline{i}\ldots\overline{q}\rangle = \sum_i 2h_{ii} + h_{pp} + h_{qq} + \left(\sum_i ii + pp\middle|\sum_j jj + qq\right) \quad (34)$$

$$\langle\Psi_{o\overline{o}}^{p\overline{q}}|H|\Psi_{o\overline{o}}^{q\overline{p}}\rangle = \langle\ldots i\ldots p\ldots\overline{i}\ldots\overline{q}|H|\ldots i\ldots q\ldots\overline{i}\ldots\overline{p}\rangle = \sum_i 2h_{ii}\langle p|q\rangle^2 + 2h_{pq}\langle p|q\rangle + \left(\sum_i ii\langle p|q\rangle + pq\middle|\sum_j jj\langle p|q\rangle + pq\right) \quad (35)$$

Here, $(\sum_i ii + pp|\sum_j jj + qq)$ and $(\sum_i ii\langle p|q\rangle + pq|\sum_j jj\langle p|q\rangle + pq)$ are shorthand notation for coulomb integrals (without exchange), e.g., $(\sum_i ii + pp|\sum_j jj + qq)$ can be expanded as: $(\sum_{ij}(ii|jj) + \sum_i(ii|qq) + \sum_j(pp|jj) + (pp|qq)$. Furthermore, this

https://doi.org/10.1021/acs.jctc.2c00740
J. Chem. Theory Comput. XXXX, XXX, XXX−XXX

expression can be simplified using E_{RHF} as a reference. Recall that the RHF energy is

$$E_{\mathrm{RHF}} = \sum_i 2h_{ii} + \sum_{ij} (ii|jj) + 2h_{oo} + 2\sum_i (ii|oo) + (oo|oo) \tag{36}$$

If we then define Fock operators as

$$\begin{aligned} f_{oo} &= h_{oo} + \sum_i (ii|oo) + (oo|oo) \\ f_{pp} &= h_{pp} + \sum_i (ii|pp) + (oo|pp) \\ f_{qq} &= h_{qq} + \sum_i (ii|qq) + (oo|qq) \\ f_{pq} &= h_{pq} + \sum_i (ii|pq) + (oo|pq) \end{aligned} \tag{37}$$

then the poCOOS-HF energy becomes:

$$\begin{aligned} \langle \Phi_{\mathrm{poCOOS-HF}}|H|\Phi_{\mathrm{poCOOS-HF}}\rangle &= E_{\mathrm{RHF}} - 2f_{oo} + (oo|oo) \\ &+ \frac{1}{1+\langle p|q\rangle^2}[f_{pp} + f_{qq} + 2f_{pq}\langle p|q\rangle + 2(pp|qq)] \\ &- \frac{1}{1+\langle p|q\rangle^2}[(oo|pp) + (oo|qq) + 2(oo|pq)\langle p|q\rangle] \end{aligned} \tag{38}$$

Once the gradient is obtained (see Appendix B for a complete derivation of the analytical energy gradient), one can use a Lagrange multiplier and a quasi-Newton method to minimize the objective function. To write the equations more succinctly, let us use the symbol x to represent a generic variable in the poCOOS-HF variable space in eq 24 formed by the set

$$\{\{c_i\}, d_o, \{d_a\}, \tilde{d}_o, \{\tilde{d}_b\}\} \tag{39}$$

The Lagrangian operator can then be written as

$$\min \mathcal{L}(x) = E_{\mathrm{poCOOS-HF}}(x) - \lambda_1 C_1(x) - \lambda_2 C_2(x) - \lambda_3 C_3(x) \tag{40}$$

where λ_1, λ_2, λ_3 are Lagrange multipliers and the three constraints are

$$\begin{aligned} C_1(x) &= \sum_i c_i^2 - 1 \\ C_2(x) &= d_o^2 + \sum_a d_a^2 - 1 \\ C_3(x) &= \tilde{d}_o^2 + \sum_b \tilde{d}_b^2 - 1 \end{aligned} \tag{41}$$

Just as one would solve for an unconstrained objective function, we use a Newton iteration to solve for the present Lagrangian (the so-called Newton-KKT equation)[35]

$$\begin{bmatrix} \nabla_{xx}^2 \mathcal{L}_k & -\nabla C_1(x_k) & -\nabla C_2(x_k) & -\nabla C_3(x_k) \\ \nabla C_1^T(x_k) & 0 & 0 & 0 \\ \nabla C_2^T(x_k) & 0 & 0 & 0 \\ \nabla C_3^T(x_k) & 0 & 0 & 0 \end{bmatrix} \begin{bmatrix} p_k \\ \lambda_{1k} \\ \lambda_{2k} \\ \lambda_{3k} \end{bmatrix} = \begin{bmatrix} -\nabla E_{\mathrm{poCOOS-HF}}(x_k) \\ -C_1(x_k) \\ -C_2(x_k) \\ -C_3(x_k) \end{bmatrix} \tag{42}$$

Here, p_k is the walking direction for x_k, i.e. $x_{k+1} = x_k + \alpha p_k$ and the step length α is obtained from a line search. To reduce the computational cost, the hessian $\nabla_{xx}^2 L$ is also approximated and updated by a BFGS scheme. In practice, for the problems below and with a reasonable starting guess, we require roughly ten cycles (i.e. line searches).

3. RESULTS AND DISCUSSION

In this paper, our goal is to compare the ground state properties (electron populations and energy) as predicted by the methods (CHF/NOCI and poCOOS-HF) above and to assess their power for propagating adiabatic dynamics; in a future publication, we will address excited state properties (and e.g., we will benchmark against the ROKS method[36,37]) so that we can assess running nonadiabatic dynamics. For the present case, because we focus on ground state theory, it is fairly straightforward to compare our results against NRG theory, which recovers only electron populations (not the total energy which would depend on the number of discrete orbitals in the bath). We will also benchmark our results against RHF and UHF.

Because molecules are very diverse and their properties can cover a multitude of chemisorption and physisorption regimes, we will test the algorithms above in three different onsite repulsion regimes: weak metal-molecule coupling $U = 10\Gamma$, intermediate coupling $U = 5\Gamma$ and strong coupling $U = \Gamma$. Figure 2 plots the ground state spin-up electron population on impurity site 1. We set the two impurity energies equal to each other, that is $\epsilon_d \equiv \epsilon_{d_1} = \epsilon_{d_2}$. The onsite energy ϵ_d (which is varied along the x-axis) can be considered a charge transfer coordinate. Each plot is separated into two ϵ_d regimes, where the total number of electrons on the impurities ranges from 4 electrons to 2 electrons and 2 electrons to 0 electrons, respectively; note that $\langle n_{\mathrm{tot}}\rangle = 4\langle n_{1\uparrow}\rangle$ for this restricted system. In the following context, these two regimes will be represented as $4 \geq \langle n_{\mathrm{tot}}\rangle \geq 2$ and $2 \geq \langle n_{\mathrm{tot}}\rangle \geq 0$. The black line is the exact NRG results for benchmark. The light blue line is restricted Hartree−Fock (RHF). The dark blue line is the unrestricted Hartree−Fock (UHF) result. The red line is constrained Hartree−Fock with non-orthogonal configuration interaction (CHF/NOCI). And lastly, the green line is the partially optimized closed-or-open shell Hartree−Fock (poCOOS-HF) result.

To begin with, consider the performance of the RHF and UHF methods. As one can see in Figure 2c, for the strong coupling regime, where static correlation is minimal, RHF itself is already a reasonable approximation to the ground state. However, for the weak or intermediate metal-molecule coupling regime, RHF becomes qualitatively incorrect when static

https://doi.org/10.1021/acs.jctc.2c00740
J. Chem. Theory Comput. XXXX, XXX, XXX−XXX

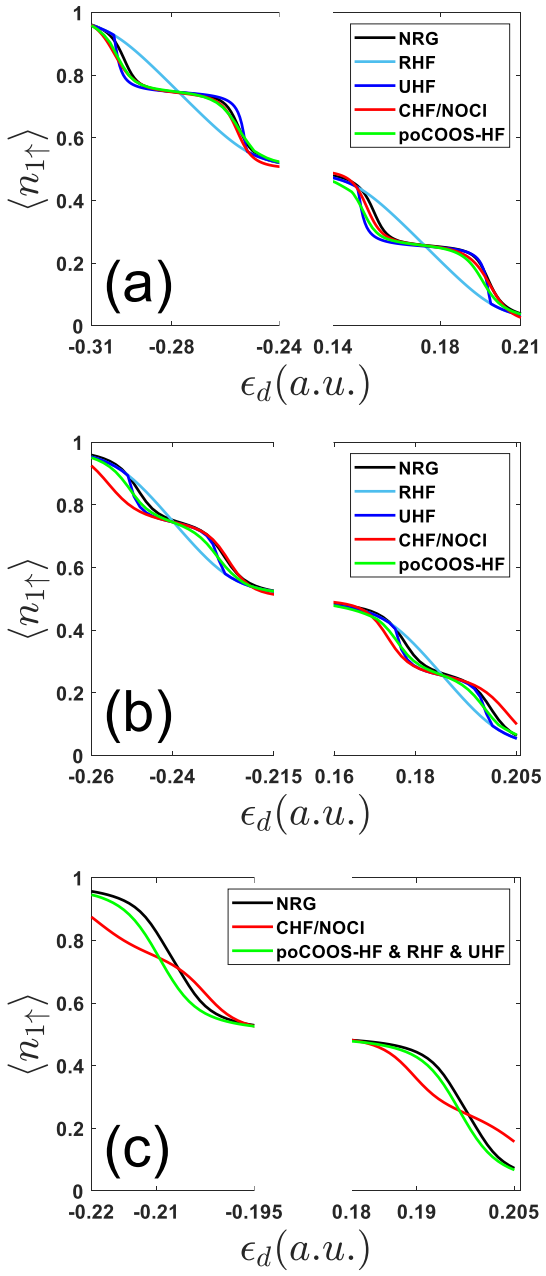

Figure 2. Ground state spin-up electron population on impurity site 1 as a function of the onsite energy $\epsilon_d = \epsilon_{d_1} = \epsilon_{d_2}$, with different onsite repulsion energies. (a) $U = 10\Gamma$; (b) $U = 5\Gamma$; (c) $U = \Gamma$. Note that poCOOS-HF results match NRG results well for all three different onsite repulsion U regimes. Here, the parameters are: $t_d = 0.2$, 803 number of states (801 bath states plus 2 impurities) with band width 0.8 and $\Gamma = 0.01$.

correlation begins to dominate. At this point, UHF does agree pretty well with NRG—but with two obvious disadvantages. First, there is a large discontinuity in the UHF results at the Coulson−Fischer point (see Figure 2a,b). Second, there is a spin-contamination problem (which will be discussed in detail in Section 4.1).

Next, we turn to the CHF/NOCI method. As is well known, one of the disadvantages of CHF(or CDFT) is that the method can fail to describe strongly coupled molecule-metal systems if the constrained subsystem (in this paper, the two impurity sites) and the unconstrained subsystem (in this paper, the bath) are difficult to distinguish. Thus, the most important test of such a system for CHF/NOCI will be the strong hybridization case. As can be seen in Figure 2, while CHF/NOCI (the red line) matches up with NRG pretty well in the weak coupling ($U = 10\Gamma$) regime, the method fails in the intermediate coupling ($U = 5\Gamma$) regime and the strong coupling ($U = \Gamma$) regime.

Lastly, let us address the green curve in Figure 2, representing the partially optimized COOS-HF (poCOOS-HF) results. As can be seen in Figure 2, poCOOS-HF results match with NRG results fairly well in the three different coupling regimes. As one would hope, in the weak and intermediate coupling regimes, poCOOS-HF behaves like UHF but with no spin-contamination; whereas in the strong coupling regime, poCOOS-HF follows the (smooth) RHF solution. As a side note, we mention that, in Figure 2c, where the coupling is so strong that RHF and UHF can be considered close to the exact solution, most of the small offset between the RHF/UHF/poCOOS-HF results and the NRG results can be attributed to the small systematic error of the NRG method (related to the choice of chain length, logarithmic discretization parameter, temperature parameter and energy truncation[23]). (For instance, the NRG approach will not be exactly on top of the RHF line even for $\Gamma = 0$, where RHF is truly exact.) These results are encouraging for future dynamics simulations.

Next, we consider energies. Figure 3 plots the ground state energy (relative to RHF) as calculated by UHF, CHF/NOCI and poCOOS-HF in three different coupling regimes: (a) $U = 10\Gamma$, (b) $U = 5\Gamma$ and (c) $U = \Gamma$. The x axis is the same as in Figure 2. One can see from Figure 3 that the poCOOS-HF energy is very close to UHF and even lower than UHF when $U = 5\Gamma$. Both UHF and poCOOS-HF give a maximum energy correction when $\langle n_{tot}\rangle = 3$ and $\langle n_{tot}\rangle = 1$, in which case the impurity has open-shell singlet character. Interestingly, in Figure 3a, even though the CHF/NOCI energy is about 1×10^{-3} higher than UHF or poCOOS-HF, the CHF/NOCI electron population (in Figure 2a) is still pretty close to the UHF and poCOOS-HF results.

4. DISCUSSION

4.1. Spin-Contamination. One of the strengths of the poCOOS-HF method is that the method works with a singlet wavefunction, and therefore the method does not have any spin-contamination. By contrast, as is well known, UHF suffers from substantial spin contamination. In Figure 4, we report spin-contamination ($\langle S^2\rangle$) for the three different onsite repulsions U. One can see that for $U = 5\Gamma$ and $U = 10\Gamma$, $\langle S^2\rangle$ for UHF can be as large as one; large changes in spin contamination arise near the UHF Coulson−Fischer points.

As a practical matter, the poCOOS-HF ansatz was designed to avoid the two problems just listed. Our goal was to seek the simplest spin-pure wavefunction method that could break symmetry (and introduce multi-reference character) in the weak and intermediate coupling regimes, but at the same time recover symmetry in the strong coupling limit, all the while being as smooth as possible. For that goal, the two standard candidates in the literature would be: broken symmetry UHF (BS-UHF) and spin-flip (SF) methods. It will be interesting to benchmark the results here versus those approaches in the future. However, already we know that the BS-UHF method is not free of spin contamination. As for spin-flip methods, often one must include more configurations than a standard SF-CIS calculation[38−40] if one wishes to recover a solution free of spin-contamination, for

https://doi.org/10.1021/acs.jctc.2c00740
J. Chem. Theory Comput. XXXX, XXX, XXX−XXX

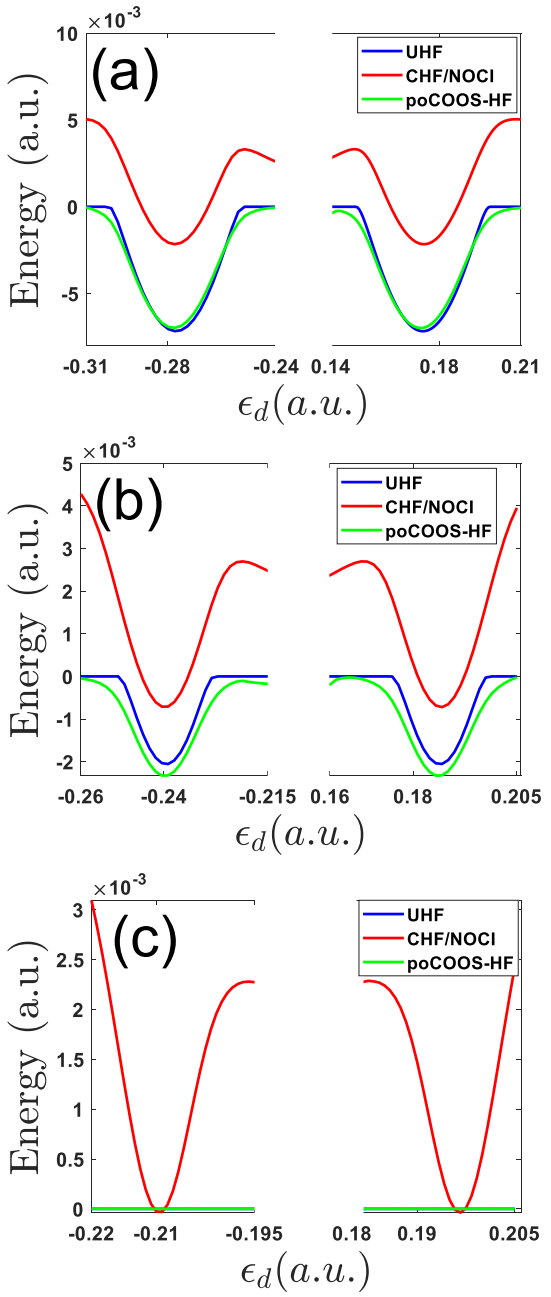

Figure 3. Ground state energy (relative to RHF energy) as a function of the onsite energy ϵ_d, with different onsite repulsion energies. (a) $U = 10\Gamma$; (b) $U = 5\Gamma$; (c) $U = \Gamma$. Note that the poCOOS-HF energy is comparable to the UHF energy for all three different onsite repulsion U regimes. All parameters are the same as in Figure 2.

example one can implement the SA-SF-CIS method of Zhang and Herbert[41] or the SF-XCIS method of Casanova and Head-Gordon.[42] Another interesting option to explore in the future would be Holomorphic Hartree−Fock[43,44] theory where smooth energy curves can be obtained, at least for systems not too large.

4.2. poCOOS Versus foCOOS Versus CASSCF(2,2). At this point, we have seen the poCOOS approach can perform fairly well for the Anderson embedding problem. That being said, one can argue that poCOOS-HF is only a partially optimized theory. After all, the algorithm optimizes only 3-orbitals ($\boldsymbol{o}, \boldsymbol{p}, \boldsymbol{q}$ in eq 24) while the remaining orbitals are kept in the RHF reference state. In particular, poCOOS-HF optimizes the orbital $\boldsymbol{o}$ within the RHF occupied space, and the remaining core orbitals are not fully optimized in terms of energy as a function orbital rotation parameters. (If we imagine the rotation of orbitals to be $e^{-\kappa}$, then κ_{it} and κ_{ia} are zero, where i indexes core orbitals, t indexes active orbitals and a indexes virtual orbitals.)

In the future, one can imagine fully optimizing all of the orbitals in the wavefunction of eq 18, what we might call a fully optimized foCOOS-HF, which optimizes a set of orthogonal orbitals (parametrized by κ_{rs}, where r, s index any orbitals) and CI coefficients (parametrized by α, β, γ in eq 32). In this spirit, one can clearly ascertain that the foCOOS ansatz would generate many (but not all) configurations suggested by a CASSCF(2,2) wavefunction. Note that this equivalence is not exact because the parameter space for CASSCF(2,2) CI coefficients is a complete ellipsoid while the parameter space for foCOOS-HF is only a subset of such a CASSCF(2,2) space. To see this constraint clearly, consider eq 32, where the normalization constraint can be written as

$$\alpha^2 + \beta^2 + 2\gamma^2 = 1 \tag{43}$$

This equation can be recast as

$$(\alpha + \beta)^2 + 2\gamma^2 - 2\alpha\beta = 1 \tag{44}$$

Note that

$$2\gamma^2 - 2\alpha\beta = 2\frac{\cos^2\theta \sin^2\eta + \sin^2\theta \cos^2\eta}{N} \geq 0 \tag{45}$$

so that our COOS-HF ansatz must satisfy

$$(\alpha + \beta)^2 \leq 1 \tag{46}$$

See Figure 5. Thus, one can consider the parameter space for foCOOS as an ellipsoid cut by two planes, $\alpha + \beta = -1$ and $\alpha + \beta = 1$, which is only a subset of the CAS space. For instance, if one considers the CAS parameter set $\left\{\alpha = \beta = \frac{1}{\sqrt{2}}, \gamma = 0\right\}$, clearly there is no corresponding $\{\theta, \eta\}$ COOS-HF parameter set.

While one might argue that this limitation represents a failure of the COOS-HF wavefunction (because a bigger variational space is always better), we are hopeful that this will not be the case. First, because we have fewer degrees of freedom, we are hopeful that with a foCOOS-HF wavefunction (as constructed exclusively from a set of meaningful orbitals), we will be able to build a balanced reference for ground and excited state calculations *without state averaging*. Second, we are also hopeful that using our choice of frontier orbitals, future work with non-orthogonal configuration interaction Hamiltonians (for excited states) will require smaller diagonalizations and few multi-reference problems. Third, we are also hopeful that with fewer degrees of freedom, there will be fewer discontinuities to deal with dynamically (and in particular, the code can be run without manually choosing an active space).

As an example of a situation we might expect to encounter, consider the case where we expect the wavefunction to have a half occupation for highest occupied molecular orbital (HOMO) and a half occupation for the lowest unoccupied molecular orbital (LUMO), in other words a one-electron density matrix D of the form

$$D = \sum_{i\in\text{core}} |i\rangle\langle i| + \frac{1}{2}|h\rangle\langle h| + \frac{1}{2}|l\rangle\langle l| \tag{47}$$

https://doi.org/10.1021/acs.jctc.2c00740
J. Chem. Theory Comput. XXXX, XXX, XXX−XXX

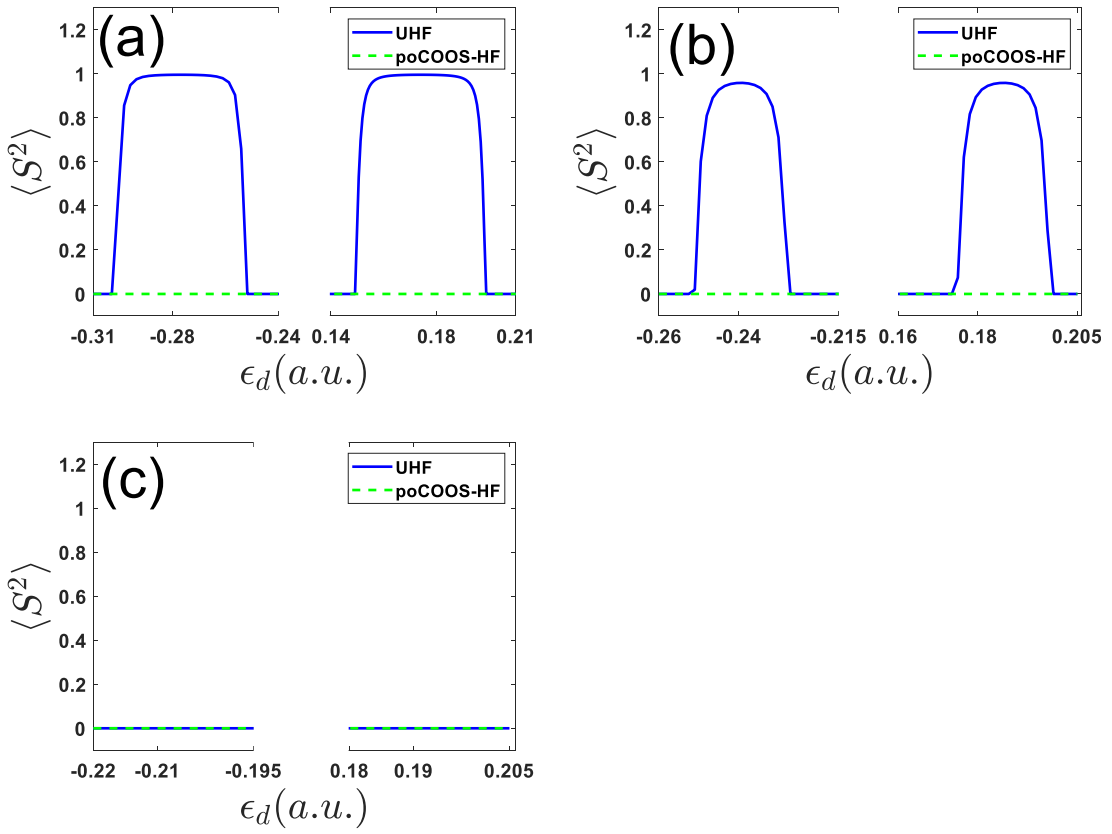

Figure 4. Spin contamination ($\langle S^2 \rangle$) as a function of the onsite energy ϵ_d with different onsite repulsion energies. (a) $U = 10\Gamma$; (b) $U = 5\Gamma$; (c) $U = \Gamma$. Note that UHF has substantial spin-contamination for $U = 5\Gamma$ and $U = 10\Gamma$. Also note that poCOOS-HF has no spin-contamination because the algorithm works with a pure singlet wavefunction, see eq 22. All parameters are the same as in Figure 2.

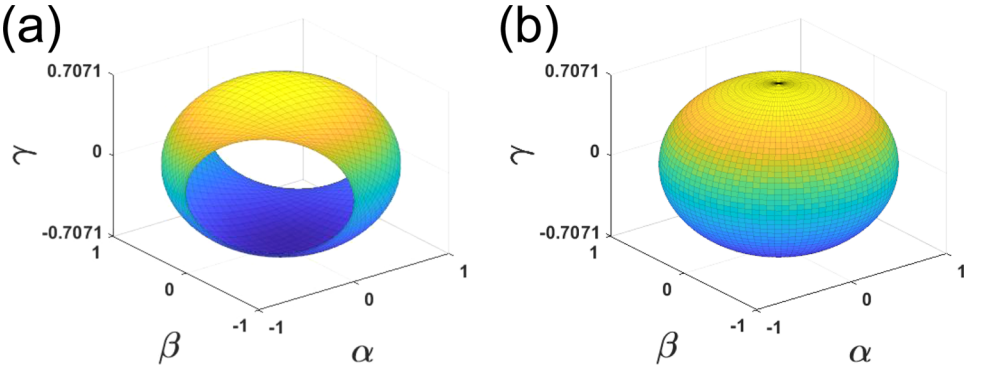

Figure 5. CI coefficients parameter space for (a) COOS-HF; (b) CASSCF(2,2). Note that the CASSCF(2,2) parameter space forms a complete ellipsoid ($\alpha^2 + \beta^2 + 2\gamma^2 = 1$) with semi-axes of $(1,1,\frac{1}{\sqrt{2}})$ while COOS-HF covers just a part of this ellipsoid. The forbidden part of the COOS-HF parameter space corresponds to the areas $\{\alpha > 0, \beta > 0\}$ and $\{\alpha < 0, \beta < 0\}$.

In order to represent such a density matrix within a CAS parameter space, there are two possible wavefunctions: $\left\{\alpha = \beta = 0, \gamma = \frac{1}{\sqrt{2}}\right\}$ $\left(\frac{1}{\sqrt{2}}(|h\bar{l}\rangle + |l\bar{h}\rangle)\right)$ and $\left\{\alpha = \beta = \frac{1}{\sqrt{2}}, \gamma = 0\right\}$ $\left(\frac{1}{\sqrt{2}}(|h\bar{h}\rangle + |l\bar{l}\rangle)\right)$. In the future, it will be interesting to check if CAS calculations converge to the same minimum starting from these two different guesses. That being said, since the parameter set $\left\{\alpha = \beta = \frac{1}{\sqrt{2}}, \gamma = 0\right\}$ is out of the COOS-HF parameter space, foCOOS will only have one unique guess wavefunction, that is, $\frac{1}{\sqrt{2}}(|h\bar{l}\rangle + |l\bar{h}\rangle)$, and so is less likely to suffer multiple solutions. In short, the essence of the present approach is that we are willing to deal with less accuracy (i.e. not including a full CAS space) if our goal is really to run nonadiabatic dynamics over a smooth and qualitatively correct surface.

This same reasoning explains why some dynamicists over prefer CASCI to CASSCF for many applications.[45]

5. CONCLUSIONS

In summary, we have presented a straightforward closed or open shell HF approach for electronic structure theory and we have compared such an approach against a CHF/NOCI ansatz for the

https://doi.org/10.1021/acs.jctc.2c00740
J. Chem. Theory Comput. XXXX, XXX, XXX−XXX

two-site Anderson model of a molecule sitting on a metal surface. We have tested the algorithms in the weak ($U = 10\Gamma$), intermediate ($U = 5\Gamma$) and strong ($U = \Gamma$) coupling regimes and we have found that poCOOS-HF can obtain accurate results as compared with exact NRG theory, recovering charge transfer states where appropriate; in particular, in the weak and intermediate coupling regimes, poCOOS-HF can recover the strong open-shell singlet character (when $\langle n_{tot}\rangle = 3$ and $\langle n_{tot}\rangle = 1$) exhibited by the impurity.

Looking forward, the COOS-HF approach has the attractive feature that the algorithm can be completely characterized by a set of orbitals, that is one does not need to list any CI coefficients. As such, the ansatz may prove amenable to a merger with DFT. Moreover, in the future, one would like to run molecular non-adiabatic dynamics on metal surfaces through the current framework. Progress on this front will depend on two important future developments. First, if one looks very carefully at Figure 2a, in the strong U regime, poCOOS-HF would appear to have four small discontinuities around $\epsilon = -0.30, -0.25, 0.15, 0.20$, attributable to a Coulson−Fischer point (similar to UHF). The changes in slope are clearly far smaller for poCOOS-HF than for UHF, but they may be unavoidable. One would hope that, if one implements the foCOOS-HF approach, such a discontinuity will be removed entirely. Second, in the future, it will be essential to generate excited states on top of a COOS-HF reference. Again, it will be essential to generate smooth surfaces as much as possible. Despite these concerns, all indications are that the present approach has the potential to be applied to reasonably sized electronic subsystems interacting with large electronic baths for use in future dynamical approaches.

APPENDIX

A. Non-Orthogonal Configuration Matrix Elements

Under the framework of constrained Hartree−Fock, suppose we find two ground states with the total number of electrons on the impurities equal to 0 and 1, denoted as

$$\left\langle \Phi_g \middle| \sum_\sigma d_{1\sigma}^\dagger d_{1\sigma} + d_{2\sigma}^\dagger d_{2\sigma} \middle| \Phi_g \right\rangle = 1$$

and

$$\left\langle \Phi'_g \middle| \sum_\sigma d_{1\sigma}^\dagger d_{1\sigma} + d_{2\sigma}^\dagger d_{2\sigma} \middle| \Phi'_g \right\rangle = 0$$

The quantity that we want to calculate is the matrix element: $\langle \Phi_g | H | \Phi'_g \rangle$. In the following paragraph, the one electron operator $d^\dagger b$ will be used to derive such non-orthogonal matrix elements; here, $d^\dagger$ represents an impurity atomic orbital and $b^\dagger$ represents a bath atomic orbital or an impurity atomic orbital.

The matrix element we wish to calculate can be explicitly written as: $\left\langle \Phi_g \middle| \sum_b \sum_\sigma d_{1\sigma}^\dagger b_\sigma + c.c. \middle| \Phi'_g \right\rangle$. For restricted orbitals, we can ignore the summation over spin σ and focus on $\left\langle \Phi_g \middle| 2 \sum_b d_1^\dagger b + c.c. \middle| \Phi'_g \right\rangle$. This equation arises by inserting an identity: $I = |\Phi_g\rangle\langle\Phi_g| + \sum_i^a |\Phi_i^a\rangle\langle_i^a|$. Since the reference state interacts only with single excitation states through a one-electron operator, the inserted identity does not need to include double or higher order excitation configurations.

$$\left\langle \Phi_g \middle| \sum_b d_1^\dagger b \middle| \Phi'_g \right\rangle = \left\langle \Phi_g \middle| \sum_b d_1^\dagger b \middle| \Phi_g \right\rangle \langle \Phi_g | \Phi'_g \rangle + \sum_{ia} \left\langle \Phi_g \middle| \sum_b d_1^\dagger b \middle| \Phi_i^a \right\rangle \langle \Phi_i^a | \Phi'_g \rangle \tag{48}$$

First of all, using second quantization, it is clear that

$$\left\langle \Phi_g \middle| \sum_b d_1^\dagger b \middle| \Phi_g \right\rangle = \sum_b \sum_i^{occ} \langle d_1 | i \rangle \langle i | b \rangle \tag{49}$$

$$\left\langle \Phi_g \middle| \sum_b d_1^\dagger b \middle| \Phi_i^a \right\rangle = \sum_b \langle d_1 | i \rangle \langle a | b \rangle \tag{50}$$

Second, let us calculate the overlap

$$\langle \Phi_g | \Phi'_g \rangle = \det(S^o) \tag{51}$$

Here, S^o is the N_o by N_o occupied orbital overlap matrix (where N_o is the number of occupied orbitals). To calculate the overlap $\langle \Phi_i^a | \Phi'_g \rangle$, we need to introduce a biorthogonal basis set. If we perform a singular value decomposition on the (occupied−occupied) S^o and (virtual−virtual) S^v overlap matrices

$$S^o = U^o \Lambda^o V^{o\dagger} \tag{52}$$

$$S^v = U^v \Lambda^v V^{v\dagger} \tag{53}$$

then the molecular orbitals can be expressed in this biorthogonal basis set

$$|i\rangle = \sum_k^{occ} |\tilde{k}\rangle U_{ik}^{o*} \tag{54}$$

$$|a\rangle = \sum_c^{vir} |\tilde{c}\rangle U_{ac}^{v*} \tag{55}$$

$$|i'\rangle = \sum_k^{occ} |\widetilde{k'}\rangle V_{ik}^{o*} \tag{56}$$

$$|a'\rangle = \sum_c^{vir} |\widetilde{c'}\rangle V_{ac}^{v*} \tag{57}$$

We can then express the overlap in this basis of biorthogonal orbitals

$$\begin{aligned} \langle \Phi_i^a | \Phi'_g \rangle &= \textstyle\sum_k^{occ} \sum_c^{vir} U_{ac}^v U_{ik}^{o*} \langle \Phi_{\tilde{k}}^{\tilde{c}} | \Phi'_{\tilde{g}} \rangle \\ &= \textstyle\sum_k^{occ} \sum_c^{vir} U_{ac}^v U_{ik}^{o*} \det(S^o) \langle \tilde{c} | \widetilde{k'} \rangle \lambda_k^{-1} \\ &= \textstyle\sum_k^{occ} U_{ik}^{o*} \det(S^o) \langle a | \widetilde{k'} \rangle \lambda_k^{-1} \end{aligned} \tag{58}$$

The second equality uses the fact that $\det(S^o) = \langle \Phi_g | \Phi'_g \rangle = \langle \Phi_{\tilde{g}} | \Phi'_{\tilde{g}} \rangle = \Pi_k^{occ} \lambda_k$ with λ_k being the diagonal element of Λ^o.

Next, the expression above can be simplified again using the identity

https://doi.org/10.1021/acs.jctc.2c00740
J. Chem. Theory Comput. XXXX, XXX, XXX−XXX

$$\sum_{k}^{\mathrm{occ}} U_{ik}^{\mathrm{o}*}\frac{1}{\lambda_k}|\tilde{k}'\rangle = \sum_{kl}^{\mathrm{occ}} U_{ik}^{\mathrm{o}*}\frac{\delta_{kl}}{\lambda_k}|\tilde{l}'\rangle = \sum_{klm}^{\mathrm{occ}} U_{ik}^{\mathrm{o}*}\frac{1}{\lambda_k}(V^{\mathrm{o}*\dagger})_{km}V_{ml}^{\mathrm{o}*}|\tilde{l}'\rangle$$
$$= \sum_{km}^{\mathrm{occ}} U_{ik}^{\mathrm{o}*}\frac{1}{\lambda_k}(V^{\mathrm{o}*\dagger})_{km}|m'\rangle = \sum_{m}^{\mathrm{occ}}\left(V^{\mathrm{o}}\frac{1}{\Lambda^{\mathrm{o}}}U^{\mathrm{o}\dagger}\right)_{mi}|m'\rangle$$
$$= \sum_{m}^{\mathrm{occ}}(S^{\mathrm{o}})^{-1}_{mi}|m'\rangle \tag{59}$$

If we substitute eq 59 into 58, we find

$$\langle\Phi_i^a|\Phi'_g\rangle = \det(S^{\mathrm{o}})\sum_{m}^{\mathrm{occ}}(S^{\mathrm{o}})^{-1}_{mi}\langle a|m'\rangle \tag{60}$$

Finally, by combining eqs 49 and 51, we evaluate the first term of eq 48.

$$\left\langle\Phi_g\middle|\sum_b d_1^\dagger b\middle|\Phi_g\right\rangle\langle\Phi_g|\Phi'_g\rangle = \det(S^{\mathrm{o}})\sum_{b\in\mathrm{bath}}\sum_{i}^{\mathrm{occ}}\langle d_1|i\rangle\langle i|b\rangle \tag{61}$$

And by combining eqs 50 and 60, we can also evaluate the second term of eq 48.

$$\sum_{ia}\left\langle\Phi_g\middle|\sum_b d_1^\dagger b\middle|\Phi_i^a\right\rangle\langle\Phi_i^a|\Phi'_g\rangle$$
$$= \det(S^o)\sum_{ia}\sum_{b}\langle d_1|i\rangle\langle a|b\rangle\sum_{m}^{occ}(S^o)^{-1}_{mi}\langle a|m'\rangle$$
$$= \det(S^o)\sum_{b}\sum_{ia}\sum_{m}^{occ}\langle b|a\rangle\langle a|m'\rangle(S^o)^{-1}_{mi}\langle i|d_1\rangle$$
$$= \det(S^o)\sum_{b}\sum_{i}\sum_{m}^{occ}\langle b|m'\rangle(S^o)^{-1}_{mi}\langle i|d_1\rangle$$
$$-\det(S^o)\sum_{b}\sum_{i}^{occ}\langle b|i\rangle\langle i|d_1\rangle \tag{62}$$

The third equality uses the property that

$$\sum_{a}^{\mathrm{vir}}|a\rangle\langle a| = I - \sum_{j}^{\mathrm{occ}}|j\rangle\langle j| \tag{63}$$

$$\sum_{m}^{\mathrm{occ}}\langle j|m'\rangle(S^{\mathrm{o}})^{-1}_{mi} = \sum_{m}^{\mathrm{occ}}(S^{\mathrm{o}})_{jm}(S^{\mathrm{o}})^{-1}_{mi} = \delta_{ji} \tag{64}$$

Altogether, by substituting eqs 61 and 62 into 48, we recover

$$\left\langle\Phi_g\middle|\sum_b d_1^\dagger b\middle|\Phi'_g\right\rangle = \det(S^{\mathrm{o}})\sum_{b\in\mathrm{bath}}\sum_{im}^{\mathrm{occ}}\langle b|m'\rangle(S^{\mathrm{o}})^{-1}_{mi}\langle i|d_1\rangle \tag{65}$$

Now we turn to the two-electron operator contribution

$$\langle\Phi_g|d^\dagger d\overline{d^\dagger}\,\overline{d}|\Phi'_g\rangle = \langle\Phi_g|d^\dagger d(|\Phi_g\rangle\langle\Phi_g| + |\Phi_i^a\rangle\langle\Phi_i^a|)$$
$$\times(|\Phi'_g\rangle\langle\Phi'_g| + |\Phi_{j'}^{b'}\rangle\langle\Phi_{j'}^{b'}|)\overline{d^\dagger}\,\overline{d}|\Phi'_g\rangle$$
$$= \langle\Phi_g|d^\dagger d|\Phi_g\rangle\langle\Phi_g|\Phi'_g\rangle\langle\Phi'_g|\overline{d^\dagger}\,\overline{d}|\Phi'_g\rangle$$
$$+\langle\Phi_g|d^\dagger d|\Phi_g\rangle\langle\Phi_g|\Phi_{j'}^{b'}\rangle\langle\Phi_{j'}^{b'}|\overline{d^\dagger}\,\overline{d}|\Phi'_g\rangle$$
$$+\langle\Phi_g|d^\dagger d|\Phi_i^a\rangle\langle\Phi_i^a|\Phi'_g\rangle\langle\Phi'_g|\overline{d^\dagger}\,\overline{d}|\Phi'_g\rangle$$
$$+\langle\Phi_g|d^\dagger d|\Phi_i^a\rangle\langle\Phi_i^a|\Phi_{j'}^{b'}\rangle\langle\Phi_{j'}^{b'}|\overline{d^\dagger}\,\overline{d}|\Phi'_g\rangle \tag{66}$$

where i, j, a, b are dummy summation indices. Then, we define

$$n_g = \langle\Phi_g|d^\dagger d|\Phi_g\rangle$$
$$n_{g'} = \langle\Phi_{g'}|d^\dagger d|\Phi_{g'}\rangle \tag{67}$$

Then, it follows that

$$\langle\Phi_g|d^\dagger d|\Phi_g\rangle\langle\Phi_g|\Phi'_g\rangle\langle\Phi'_g|\overline{d^\dagger}\,\overline{d}|\Phi'_g\rangle = \det(S^{\mathrm{o}})n_g n_{g'}$$
$$\sum_{j'}^{\mathrm{occ}}\sum_{b'}^{\mathrm{vir}}\langle\Phi_g|d^\dagger d|\Phi_g\rangle\langle\Phi_g|\Phi_{j'}^{b'}\rangle\langle\Phi_{j'}^{b'}|\overline{d^\dagger}\,\overline{d}|\Phi'_g\rangle$$
$$= \det(S^{\mathrm{o}})n_g\sum_{ij'}^{\mathrm{occ}}\langle d|j'\rangle(S^{\mathrm{o}})^{-1}_{j'i}\langle i|d\rangle - \det(S^{\mathrm{o}})n_g n_{g'}$$
$$\sum_{i}^{\mathrm{occ}}\sum_{a}^{\mathrm{vir}}\langle\Phi_g|d^\dagger d|\Phi_i^a\rangle\langle\Phi_i^a|\Phi'_g\rangle\langle\Phi'_g|\overline{d^\dagger}\,\overline{d}|\Phi'_g\rangle$$
$$= \det(S^{\mathrm{o}})n_{g'}\sum_{ij'}^{\mathrm{occ}}\langle d|j'\rangle(S^{\mathrm{o}})^{-1}_{j'i}\langle i|d\rangle - \det(S^{\mathrm{o}})n_g n_{g'}$$
$$\sum_{ij'}^{\mathrm{occ}}\sum_{ab'}^{\mathrm{vir}}\langle\Phi_g|d^\dagger d|\Phi_i^a\rangle\langle\Phi_i^a|\Phi_{j'}^{b'}\rangle\langle\Phi_{j'}^{b'}|\overline{d^\dagger}\,\overline{d}|\Phi'_g\rangle$$
$$= \det(S^{\mathrm{o}})\sum_{im'}^{\mathrm{occ}}\langle d|m'\rangle(S^{\mathrm{o}})^{-1}_{m'i}\langle i|d\rangle\sum_{kj'}^{\mathrm{occ}}\langle d|j'\rangle(S^{\mathrm{o}})^{-1}_{j'k}\langle k|d\rangle$$
$$- \det(S^{\mathrm{o}})n_g\sum_{kj'}^{\mathrm{occ}}\langle d|j'\rangle(S^{\mathrm{o}})^{-1}_{j'k}\langle k|d\rangle$$
$$- \det(S^{\mathrm{o}})n_{g'}\sum_{im'}^{\mathrm{occ}}\langle d|m'\rangle(S^{\mathrm{o}})^{-1}_{m'i}\langle i|d\rangle + \det(S^{\mathrm{o}})n_g n_{g'} \tag{68}$$

Altogether, there is a lot of cancellation, and the two-electron operator contribution is

$$\langle\Phi_g|d^\dagger d\overline{d^\dagger}\,\overline{d}|\Phi'_g\rangle = \det(S^{\mathrm{o}})\sum_{im'}^{\mathrm{occ}}\langle d|m'\rangle(S^{\mathrm{o}})^{-1}_{m'i}\langle i|d\rangle$$
$$\sum_{kj'}^{\mathrm{occ}}\langle d|j'\rangle(S^{\mathrm{o}})^{-1}_{j'k}\langle k|d\rangle \tag{69}$$

B. Analytical Energy Gradient for poCOOS-HF

For the sake of completeness, here we list all of the electronic derivatives (with respect to orbital variations) of the relevant fock operators, overlap matrix elements, and two electron matrix elements as present in eq 38. The indices i,j,k,l represent occupied orbitals and a,b,c,d represent virtual orbitals.

https://doi.org/10.1021/acs.jctc.2c00740
J. Chem. Theory Comput. XXXX, XXX, XXX−XXX

B.1. Derivatives of Fock Operators.

$$\frac{\partial f_{oo}}{\partial c_i} = 2\sum_j c_j f_{ij} \tag{70}$$

$$\frac{\partial f_{pp}}{\partial c_i} = d_o^2 \cdot 2\sum_j c_j f_{ij} + 2\sum_a d_o d_a f_{ia}$$

$$\frac{\partial f_{pp}}{\partial d_o} = 2d_o \sum_{ij} c_i c_j f_{ij} + 2\sum_a d_a \sum_i c_i f_{ia}$$

$$\frac{\partial f_{pp}}{\partial d_a} = 2d_o \sum_i c_i f_{ia} + 2\sum_b d_b f_{ab} \tag{71}$$

$$\frac{\partial f_{qq}}{\partial c_i} = \tilde{d}_o^2 \cdot 2\sum_j c_j f_{ij} + 2\sum_a \tilde{d}_o \tilde{d}_a f_{ia}$$

$$\frac{\partial f_{qq}}{\partial \tilde{d}_o} = 2\tilde{d}_o \sum_{ij} c_i c_j f_{ij} + 2\sum_a \tilde{d}_a \sum_i c_i f_{ia}$$

$$\frac{\partial f_{qq}}{\partial \tilde{d}_a} = 2\tilde{d}_o \sum_i c_i f_{ia} + 2\sum_b \tilde{d}_b f_{ab} \tag{72}$$

$$\frac{\partial f_{pq}}{\partial c_i} = d_o \tilde{d}_o \cdot 2\sum_j c_j f_{ij} + \sum_a \tilde{d}_o d_a f_{ia} + \sum_a d_o \tilde{d}_a f_{ia}$$

$$\frac{\partial f_{pq}}{\partial d_o} = \tilde{d}_o \sum_{ij} c_i c_j f_{ij} + \sum_a \tilde{d}_a \sum_i c_i f_{ia}$$

$$\frac{\partial f_{pq}}{\partial \tilde{d}_o} = d_o \sum_{ij} c_i c_j f_{ij} + \sum_a d_a \sum_i c_i f_{ia}$$

$$\frac{\partial f_{pq}}{\partial d_a} = \tilde{d}_o \sum_i c_i f_{ia} + \sum_b \tilde{d}_b f_{ab}$$

$$\frac{\partial f_{pq}}{\partial \tilde{d}_a} = d_o \sum_i c_i f_{ia} + \sum_b d_b f_{ab} \tag{73}$$

B.2. Derivatives of Overlap Matrices.

$$\frac{\partial \langle p|q\rangle}{\partial c_i} = d_o \tilde{d}_o \cdot 2c_i + \sum_a d_o \tilde{d}_a \langle i|a\rangle + \sum_a \tilde{d}_o d_a \langle i|a\rangle$$

$$\frac{\partial \langle p|q\rangle}{\partial d_o} = \tilde{d}_o \sum_i c_i^2 + \sum_{ai} \tilde{d}_a c_i \langle i|a\rangle$$

$$\frac{\partial \langle p|q\rangle}{\partial \tilde{d}_o} = d_o \sum_i c_i^2 + \sum_{ai} d_a c_i \langle i|a\rangle$$

$$\frac{\partial \langle p|q\rangle}{\partial d_a} = \sum_b \tilde{d}_b \langle a|b\rangle + \sum_i \tilde{d}_o c_i \langle i|a\rangle$$

$$\frac{\partial \langle p|q\rangle}{\partial \tilde{d}_a} = \sum_b d_b \langle b|a\rangle + \sum_i d_o c_i \langle i|a\rangle \tag{74}$$

.

B.3. Derivatives of Two Electron Integrals.

$$\frac{\partial (oo|oo)}{\partial c_i} = 4\sum_{jkl} c_j c_k c_l (ij|kl) \tag{75}$$

$$\begin{aligned}\frac{\partial (pq|qp)}{\partial c_i} &= d_o^2 \tilde{d}_o^2 \sum_{jkl} 4c_j c_k c_l (ij|kl) \\ &+ \left(d_o^2 2\sum_a \tilde{d}_o \tilde{d}_a + 2\sum_a d_o d_a \tilde{d}_o^2\right)\sum_{jk} 3c_j c_k (ij|ka) \\ &+ \left(d_o^2 \sum_{ab} \tilde{d}_a \tilde{d}_b + 2\sum_a d_o d_a 2\sum_b \tilde{d}_o \tilde{d}_b \right. \\ &\left. + \sum_{ab} d_a d_b \cdot \tilde{d}_o^2\right)\sum_j 2c_j (ij|ab) \\ &+ \left(2\sum_a d_o d_a \sum_{bc} \tilde{d}_b \tilde{d}_c + \sum_{ab} d_a d_b 2\sum_c \tilde{d}_o \tilde{d}_c\right)(ia|bc)\end{aligned} \tag{76}$$

$$\begin{aligned}\frac{\partial (pq|qp)}{\partial d_o} &= 2d_o \tilde{d}_o^2 \sum_{ijkl} c_i c_j c_k c_l (ij|kl) \\ &+ \left(2d_o \cdot 2\sum_a \tilde{d}_o \tilde{d}_a + 2\sum_a d_a \cdot \tilde{d}_o^2\right)\cdot \sum_{ijk} c_i c_j c_k (ij|ka) \\ &+ \left(2d_o \cdot \sum_{ab} \tilde{d}_a \tilde{d}_b + 2\sum_a d_a \cdot 2\sum_b \tilde{d}_o \tilde{d}_b\right)\cdot \\ &\sum_{ij} c_i c_j (ij|ab) + \left(2\sum_a d_a \cdot \sum_{bc} \tilde{d}_b \tilde{d}_c\right)\cdot \sum_i c_i (ia|bc)\end{aligned} \tag{77}$$

$$\begin{aligned}\frac{\partial (pq|qp)}{\partial d_a} &= (2d_o \tilde{d}_o^2)\sum_{ijk} c_i c_j c_k (ij|ka) \\ &+ \left(2d_o 2\sum_b \tilde{d}_o \tilde{d}_b + \sum_b 2d_b \tilde{d}_o^2\right)\sum_{ij} c_i c_j (ij|ab) \\ &+ \left(2d_o \sum_{bc} \tilde{d}_b \tilde{d}_c + \sum_b 2d_b 2\sum_c \tilde{d}_o \tilde{d}_c\right)\sum_i c_i (ia|bc) \\ &+ \sum_b 2d_b \sum_{cd} \tilde{d}_c \tilde{d}_d (ab|cd)\end{aligned} \tag{78}$$

$$\begin{aligned}\frac{\partial (pq|qp)}{\partial \tilde{d}_o} &= 2d_o^2 \tilde{d}_o \sum_{ijkl} c_i c_j c_k c_l (ij|kl) \\ &+ \left(d_o^2 2\sum_a \tilde{d}_a + 2\sum_a d_o d_a 2\tilde{d}_o\right)\sum_{ijk} c_i c_j c_k (ij|ka) \\ &+ \left(2\sum_a d_o d_a \cdot 2\sum_b \tilde{d}_b + \sum_{ab} d_a d_b 2\tilde{d}_o\right)\sum_{ij} c_i c_j (ij|ab) \\ &+ \left(\sum_{ab} d_a d_b 2\sum_c \tilde{d}_c\right)\sum_i c_i (ia|bc)\end{aligned} \tag{79}$$

https://doi.org/10.1021/acs.jctc.2c00740
J. Chem. Theory Comput. XXXX, XXX, XXX−XXX

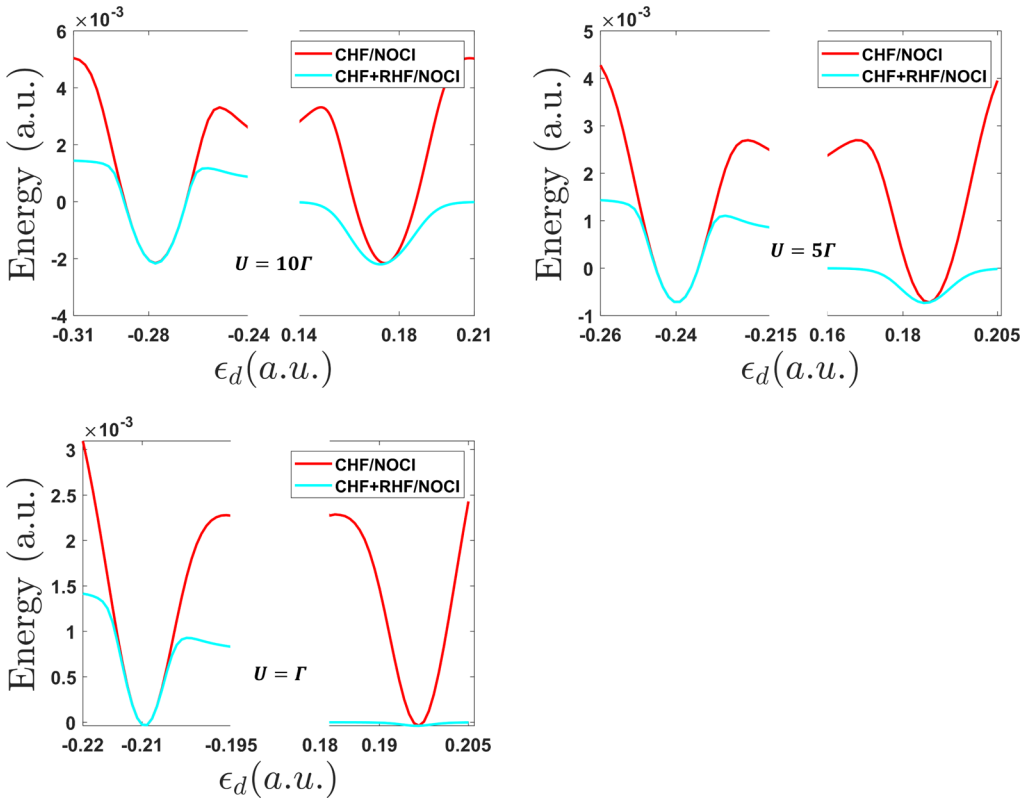

Figure 6. CHF + RHF/NOCI energy (relative to RHF energy) as a function of ϵ_d. (a) $U = 10\Gamma$; (b) $U = 5\Gamma$; (c) $U = \Gamma$. Note that including the RHF ansatz within the CI does greatly improve the NOCI energetic result. All parameters are the same as in Figure 2.

$$\frac{\partial(pq|qp)}{\partial \tilde{d}_b} = (d_o^2 \cdot 2\tilde{d}_o)\cdot \sum_{ijk} c_i c_j c_k (ijlkb) + \left(d_o^2 \cdot \sum_a 2\tilde{d}_a + 2\sum_a d_o d_a \cdot 2\tilde{d}_o\right)\cdot \sum_{ij} c_i c_j (ijlab) + \left(2\sum_a d_o d_a \cdot \sum_c 2\tilde{d}_c + \sum_{ac} d_a d_c \cdot 2\tilde{d}_o\right)\cdot \sum_i c_i (ialcb) + \sum_{ac} d_a d_c \cdot \sum_d 2\tilde{d}_a (aclbd) \tag{80}$$

$$\frac{\partial(oo|pp)}{\partial c_i} = d_o^2 \cdot \sum_{jkl} 4c_j c_k c_l (ijlkl) + 2\sum_a d_o d_a \cdot \sum_{jk} 3c_j c_k (ijlka) + \sum_{ab} d_a d_b \cdot \sum_j 2c_j (ijlab)$$

$$\frac{\partial(oo|pp)}{\partial d_o} = 2d_o \cdot \sum_{ijkl} c_i c_j c_k c_l (ijlkl) + 2\sum_a d_a \cdot \sum_{ijk} c_i c_j c_k (ijlka)$$

$$\frac{\partial(oo|pp)}{\partial d_a} = 2d_o \cdot \sum_{ijk} c_i c_j c_k (ijlka) + \sum_b 2d_b \cdot \sum_{ij} c_i c_j (ijlab) \tag{81}$$

$$\frac{\partial(oo|qq)}{\partial c_i} = \tilde{d}_o^2 \cdot \sum_{jkl} 4c_j c_k c_l (ijlkl) + 2\sum_a \tilde{d}_o \tilde{d}_a \cdot \sum_{jk} 3c_j c_k (ijlka) + \sum_{ab} \tilde{d}_a \tilde{d}_b \cdot \sum_j 2c_j (ijlab)$$

$$\frac{\partial(oo|qq)}{\partial \tilde{d}_o} = 2\tilde{d}_o \cdot \sum_{ijkl} c_i c_j c_k c_l (ijlkl) + 2\sum_a \tilde{d}_a \cdot \sum_{ijk} c_i c_j c_k (ijlka)$$

$$\frac{\partial(oo|qq)}{\partial \tilde{d}_a} = 2\tilde{d}_o \cdot \sum_{ijk} c_i c_j c_k (ijlka) + \sum_b 2\tilde{d}_b \cdot \sum_{ij} c_i c_j (ijlab) \tag{82}$$

$$\frac{\partial(oo|pq)}{\partial c_i} = d_o \tilde{d}_o \cdot \sum_{jkl} 4c_i c_j c_k c_l (ijlkl) + \sum_a (d_a \tilde{d}_o + d_o \tilde{d}_a)\cdot \sum_{jk} 3c_i c_j c_k (ijlka) + \sum_{ab} d_a \tilde{d}_b \cdot \sum_{ij} 2c_j (ijlab)$$

$$\frac{\partial(oo|pq)}{\partial d_o} = \tilde{d}_o \cdot \sum_{ijkl} c_i c_j c_k c_l (ijlkl) + \sum_a \tilde{d}_a \cdot \sum_{ijk} c_i c_j c_k (ijlka)$$

$$\frac{\partial(oo|pq)}{\partial \tilde{d}_o} = d_o \cdot \sum_{ijkl} c_i c_j c_k c_l (ijlkl) + \sum_a d_a \cdot \sum_{ijk} c_i c_j c_k (ijlka)$$

$$\frac{\partial(oo|pq)}{\partial d_a} = \tilde{d}_o \cdot \sum_{ijk} c_i c_j c_k (ijlka) + \sum_b \tilde{d}_b \cdot \sum_{ij} c_i c_j (ijlab)$$

$$\frac{\partial(oo|pq)}{\partial \tilde{d}_a} = d_o \cdot \sum_{ijk} c_i c_j c_k (ijlka) + \sum_b d_b \cdot \sum_{ij} c_i c_j (ijlab) \tag{83}$$

https://doi.org/10.1021/acs.jctc.2c00740
J. Chem. Theory Comput. XXXX, XXX, XXX−XXX

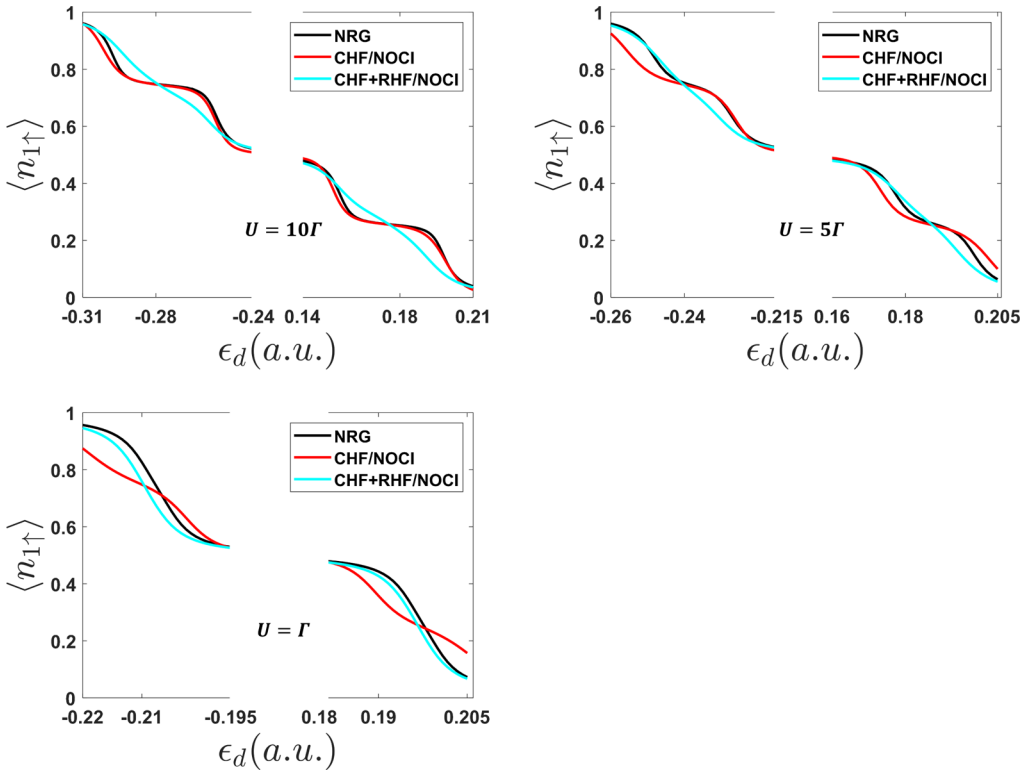

Figure 7. CHF + RHF/NOCI electronic population on site 1 as a function of ϵ_d. (a) $U = 10\Gamma$; (b) $U = 5\Gamma$; (c) $U = \Gamma$. Note that, unfortunately, including the RHF configuration in our NOCI Hamiltonian results in worse results for the electronic population because the final result now looks like the RHF result, which is good for $U = \Gamma$ but wrong for $U = 10\Gamma$. The problem at bottom is that the CHF energies are simply too large relative to the RHF energy. All parameters are the same as in Figure 2.

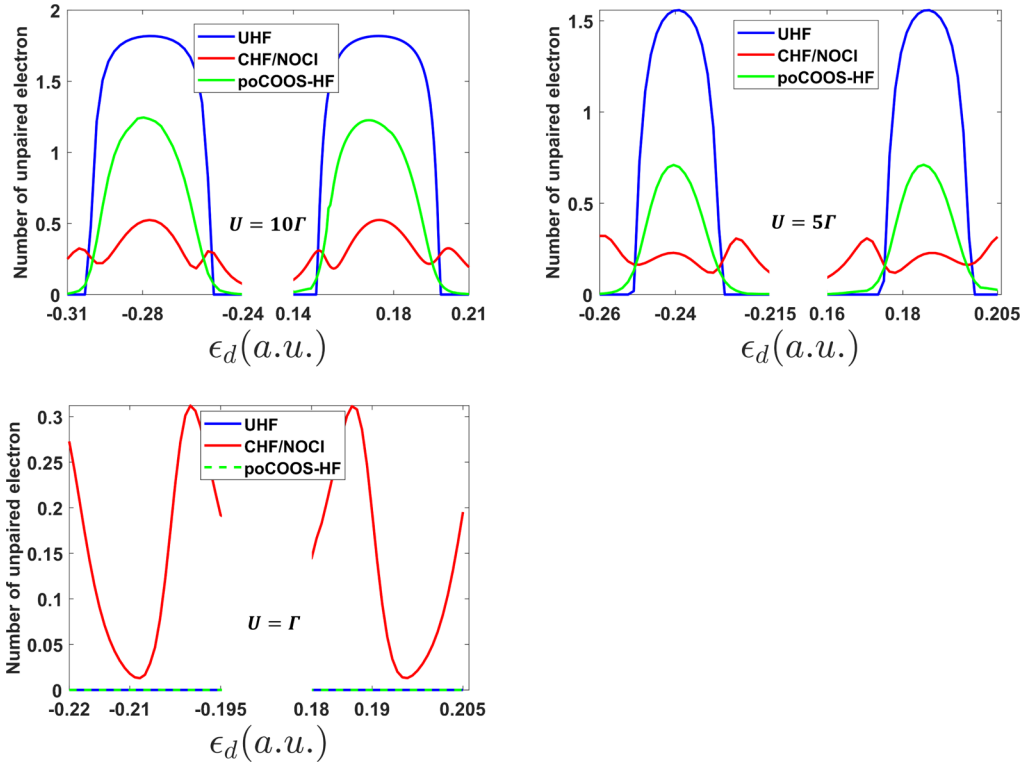

Figure 8. Number of unpaired electrons as a function of ϵ_d. (a) $U = 10\Gamma$ (here one expects two unpaired electrons); (b) $U = 5\Gamma$; (c) $U = \Gamma$ (here one expects zero unpaired electrons). While UHF performs best, poCOOS-HF does retrieve the correct trend whereas CHF/NOCI is quite inaccurate (sometimes too small, sometimes too large). All parameters are the same as in Figure 2.

https://doi.org/10.1021/acs.jctc.2c00740
J. Chem. Theory Comput. XXXX, XXX, XXX−XXX

C. Including the Restricted Hartree−Fock Configuration within the Nonorthogonal Configuration Interaction Hamiltonian (CHF + RHF/NOCI)

Above, in Section 3, we showed that a non-orthogonal CI with CHF states did not perform well for the two-site AH model. Here, we will now show how this result changes if we include the RHF configuration within the CHF/NOCI basis. In Figure 6, we plot the energy (relative to the RHF energy) of the resulting algorithms for different electron−electron repulsions (U); in Figure 7, we plot the electronic population on site 1. As one might have guessed, including the RHF ansatz within the CI does greatly improve the NOCI energy. However, this improvement comes at the cost of worse electronic population results (because the CHF + RHF/NOCI results now resemble the RHF answer, which is good for $U = \Gamma$ but wrong for $U = 10\Gamma$).

The problem (at bottom) is that the CHF/NOCI energies are just too large and not balanced with a RHF ansatz. Note that we are using restricted CHF configurations here (rather than unrestricted configurations); the energetic balance would likely be better if we used unrestricted CHF configurations (though at the cost of larger discontinuities).

D. Analysis of the Number of Unpaired Electrons

Here, in order to build intuition around the COOS approach presented above, we construct the one-particle reduced density matrix (1RDM) and calculate the number of unpaired electrons. Following ref 46, let the number of unpaired electrons n_u be

$$n_u = \sum_i^M 1 - |1 - n_i| = M - \sum_i^M |1 - n_i| \tag{84}$$

where n_i is the i-th eigenvalue of the 1RDM and M is the total number of basis functions. For n_{occ} occupied orbitals, we build the 1RDM's as follows

1 For poCOOS-HF, the 1RDM follows from the 2 by 2 density matrix within the subspace of the two active orbitals.
2 The 1RDM for UHF is: $D = \sum_i^{n_{occ}} |i\rangle\langle i| + |\bar{i}\rangle\langle\bar{i}|$.
3 The 1RDM for CHF/NOCI is: $D_{\mu\nu} = \sum_{I=0}^{4}\sum_{J=0}^{4} c_I c_J \langle\Phi_I|\mu^\dagger\nu|\Phi_J\rangle$. Here, the summation over I, J represents the $0e$, $1e$, $2e$, $3e$, $4e$ configuration states. In matrix representation, the 1RDM can be written as

$$D = \sum_{I=0}^{4}\sum_{J=0}^{4} c_I c_J C_{J,\mathrm{occ}} (S^{o}_{IJ})^{-1} C^{T}_{I,\mathrm{occ}}$$

where c_I, c_J are CI coefficients; $C_{J,\mathrm{occ}}$ is the matrix of the occupied molecular orbital coefficients for the J-th configuration and $C^T_{I,\mathrm{occ}}$ is the matrix of the occupied molecular orbital coefficients (transposed) for I-th configuration. The occupied overlap matrix is defined as: $S^{o}_{IJ} = C^T_{I,\mathrm{occ}} C_{J,\mathrm{occ}}$.

In all cases, the trace of the 1RDM is equal to the number of electrons ($2n_{occ}$).

In Figure 8, we plot the number of unpaired electrons predicted by CHF/NOCI, poCOOS-HF and UHF. Note that, in the limit that $U \gg \Gamma$, we expect to find two unpaired electrons (when the system shows open-shell character around $\epsilon_d = -0.28$ and $\epsilon_d = 0.18$). In the limit that $U \ll \Gamma$, we expect to find zero unpaired electrons. According to Figure 8, UHF performs quite well as one might expect, but poCOOS-HF does retrieve the correct trend. CHF/NOCI is not accurate at all (sometimes too small, sometimes too large). (Note again that we are using restricted CHF configurations here.) These results would suggest that the strong performance of poCOOS-HF above was not simply fortuitous; the method would appear to get the right results for the right reasons.

AUTHOR INFORMATION

Corresponding Author

Joseph Subotnik − *Department of Chemistry, University of Pennsylvania, Philadelphia, Pennsylvania 19104, United States*; Phone: +1 (215) 746-7078; Email: subotnik@sas.upenn.edu

Authors

Junhan Chen − *Department of Chemistry, University of Pennsylvania, Philadelphia, Pennsylvania 19104, United States*; orcid.org/0000-0003-4843-6324

Wenjie Dou − *School of Science, Westlake University, Hangzhou, Zhejiang 310024, China; Institute of Natural Sciences, Westlake Institute for Advanced Study, Hangzhou, Zhejiang 310024, China*; orcid.org/0000-0001-5410-6183

Complete contact information is available at: https://pubs.acs.org/10.1021/acs.jctc.2c00740

Notes

The authors declare no competing financial interest.

ACKNOWLEDGMENTS

This work was supported by the U.S. Air Force Office of Scientific Research (USAFOSR) under Grant Nos. FA9550-18-1-0497 and FA9550-18-1-0420. We thank the DoD High Performance Computing Modernization Program for computer time.

REFERENCES

(1) Kaneko, T.; Yunoki, S.; Millis, A. J. Charge stiffness and long-range correlation in the optically induced η-pairing state of the one-dimensional Hubbard model. *Phys. Rev. Res.* **2020**, *2*, 032027.

(2) Cevolani, L.; Despres, J.; Carleo, G.; Tagliacozzo, L.; Sanchez-Palencia, L. Universal scaling laws for correlation spreading in quantum systems with short-and long-range interactions. *Phys. Rev. B* **2018**, *98*, 024302.

(3) Han, Q.; Millis, A. Lattice energetics and correlation-driven metal-insulator transitions: The case of Ca2 RuO4. *Phys. Rev. Lett.* **2018**, *121*, 067601.

(4) Keshavarz, S.; Schött, J.; Millis, A. J.; Kvashnin, Y. O. Electronic structure, magnetism, and exchange integrals in transition-metal oxides: Role of the spin polarization of the functional in DFT+ U calculations. *Phys. Rev. B* **2018**, *97*, 184404.

(5) Knizia, G.; Chan, G. K.-L. Density matrix embedding: A simple alternative to dynamical mean-field theory. *Phys. Rev. Lett.* **2012**, *109*, 186404.

(6) Lee, S. J.; Welborn, M.; Manby, F. R.; Miller, T. F., III Projection-based wavefunction-in-DFT embedding. *Acc. Chem. Res.* **2019**, *52*, 1359−1368.

(7) Bulik, I. W.; Scuseria, G. E.; Dukelsky, J. Density matrix embedding from broken symmetry lattice mean fields. *Phys. Rev. B: Condens. Matter Mater. Phys.* **2014**, *89*, 035140.

(8) Bulik, I. W.; Chen, W.; Scuseria, G. E. Electron correlation in solids via density embedding theory. *J. Chem. Phys.* **2014**, *141*, 054113.

(9) Klüner, T.; Govind, N.; Wang, Y. A.; Carter, E. A. Periodic density functional embedding theory for complete active space self-consistent

field and configuration interaction calculations: Ground and excited states. *J. Chem. Phys.* **2002**, *116*, 42−54.
(10) Sharifzadeh, S.; Huang, P.; Carter, E. Embedded configuration interaction description of CO on Cu (111): Resolution of the site preference conundrum. *J. Phys. Chem. C* **2008**, *112*, 4649−4657.
(11) Libisch, F.; Huang, C.; Carter, E. A. Embedded correlated wavefunction schemes: Theory and applications. *Acc. Chem. Res.* **2014**, *47*, 2768−2775.
(12) Gavnholt, J.; Olsen, T.; Engelund, M.; Schiøtz, J. Δ self-consistent field method to obtain potential energy surfaces of excited molecules on surfaces. *Phys. Rev. B: Condens. Matter Mater. Phys.* **2008**, *78*, 075441.
(13) Bunermann, O.; Jiang, H.; Dorenkamp, Y.; Kandratsenka, A.; Janke, S. M.; Auerbach, D. J.; Wodtke, A. M. Electron-hole pair excitation determines the mechanism of hydrogen atom adsorption. *Science* **2015**, *350*, 1346−1349.
(14) Morin, M.; Levinos, N.; Harris, A. Vibrational energy transfer of CO/Cu (100): Nonadiabatic vibration/electron coupling. *J. Chem. Phys.* **1992**, *96*, 3950−3956.
(15) Huang, Y.; Rettner, C. T.; Auerbach, D. J.; Wodtke, A. M. Vibrational promotion of electron transfer. *Science* **2000**, *290*, 111−114.
(16) Raghavachari, K.; Trucks, G. W.; Pople, J. A.; Head-Gordon, M. A fifth-order perturbation comparison of electron correlation theories. *Chem. Phys. Lett.* **1989**, *157*, 479−483.
(17) Andersson, K.; Malmqvist, P. A.; Roos, B. O.; Sadlej, A. J.; Wolinski, K. Second-order perturbation theory with a CASSCF reference function. *J. Phys. Chem.* **1990**, *94*, 5483.
(18) Andersson, K.; Malmqvist, P.-Å.; Roos, B. O. Second-order perturbation theory with a complete active space self-consistent field reference function. *J. Chem. Phys.* **1992**, *96*, 1218−1226.
(19) Bruna, P.; Peyerimhoff, S. Excited-state potentials. *Ab initio methods in quantum chemistry I*; John Wiley & Sons Ltd, 1987; Vol. *1*−*98*.
(20) Sherrill, C. D.; Schaefer, H. F., III *Advances in Quantum Chemistry*; Elsevier, 1999; Vol. *34*, pp 143−269.
(21) Sherrill, C. D. *Computational Algorithms for Large-Scale Full and Multi-Reference Configuration Interaction Wavefunctions*; University of Georgia, 1996.
(22) Anderson, P. W. Localized magnetic states in metals. *Phys. Rev.* **1961**, *124*, 41.
(23) Bulla, R.; Costi, T. A.; Pruschke, T. Numerical renormalization group method for quantum impurity systems. *Rev. Mod. Phys.* **2008**, *80*, 395.
(24) Fu, W.; Sachdev, S. Numerical study of fermion and boson models with infinite-range random interactions. *Phys. Rev. B* **2016**, *94*, 035135.
(25) Gull, E.; Millis, A. J.; Lichtenstein, A. I.; Rubtsov, A. N.; Troyer, M.; Werner, P. Continuous-time Monte Carlo methods for quantum impurity models. *Rev. Mod. Phys.* **2011**, *83*, 349.
(26) Georges, A.; Kotliar, G.; Krauth, W.; Rozenberg, M. J. Dynamical mean-field theory of strongly correlated fermion systems and the limit of infinite dimensions. *Rev. Mod. Phys.* **1996**, *68*, 13.
(27) Kaduk, B.; Kowalczyk, T.; Van Voorhis, T. Constrained density functional theory. *Chem. Rev.* **2012**, *112*, 321−370.
(28) Ma, H.; Wang, W.; Kim, S.; Cheng, M.-H.; Govoni, M.; Galli, G. PyCDFT: A Python package for constrained density functional theory. *J. Comput. Chem.* **2020**, *41*, 1859.
(29) Souza, A.; Rungger, I.; Pemmaraju, C.; Schwingenschloegl, U.; Sanvito, S. Constrained-DFT method for accurate energy-level alignment of metal/molecule interfaces. *Phys. Rev. B: Condens. Matter Mater. Phys.* **2013**, *88*, 165112.
(30) Behler, J.; Delley, B.; Reuter, K.; Scheffler, M. Nonadiabatic potential-energy surfaces by constrained density-functional theory. *Phys. Rev. B: Condens. Matter Mater. Phys.* **2007**, *75*, 115409.
(31) Mavros, M. G.; Van Voorhis, T. Communication: CDFT-CI couplings can be unreliable when there is fractional charge transfer. *J. Chem. Phys.* **2015**, *143*, 231102.
(32) Jin, Z.; Dou, W.; Subotnik, J. E. Configuration interaction approaches for solving quantum impurity models. *J. Chem. Phys.* **2020**, *152*, 064105.
(33) Chen, J.; Jin, Z.; Dou, W.; Subotnik, J. Electronic Structure for Multielectronic Molecules near a Metal Surface. *J. Phys. Chem. C* **2021**, *125*, 2884−2899.
(34) Wu, Q.; Van Voorhis, T. Direct optimization method to study constrained systems within density-functional theory. *Phys. Rev. A: At., Mol., Opt. Phys.* **2005**, *72*, 024502.
(35) Wright, S.; Nocedal, J.; et al. Numerical optimization. *Springer Sci.* **1999**, *35*, 7.
(36) Filatov, M.; Shaik, S. A spin-restricted ensemble-referenced Kohn−Sham method and its application to diradicaloid situations. *Chem. Phys. Lett.* **1999**, *304*, 429−437.
(37) Kowalczyk, T.; Tsuchimochi, T.; Chen, P.-T.; Top, L.; Van Voorhis, T. Excitation energies and Stokes shifts from a restricted open-shell Kohn-Sham approach. *J. Chem. Phys.* **2013**, *138*, 164101.
(38) Alguire, E.; Subotnik, J. E. Diabatic couplings for charge recombination via Boys localization and spin-flip configuration interaction singles. *J. Chem. Phys.* **2011**, *135*, 044114.
(39) Krylov, A. I. Spin-flip configuration interaction: an electronic structure model that is both variational and size-consistent. *Chem. Phys. Lett.* **2001**, *350*, 522−530.
(40) Shao, Y.; Head-Gordon, M.; Krylov, A. I. The spin−flip approach within time-dependent density functional theory: Theory and applications to diradicals. *J. Chem. Phys.* **2003**, *118*, 4807−4818.
(41) Zhang, X.; Herbert, J. M. Spin-flip, tensor equation-of-motion configuration interaction with a density-functional correction: A spin-complete method for exploring excited-state potential energy surfaces. *J. Chem. Phys.* **2015**, *143*, 234107.
(42) Casanova, D.; Head-Gordon, M. The spin-flip extended single excitation configuration interaction method. *J. Chem. Phys.* **2008**, *129*, 064104.
(43) Hiscock, H. G.; Thom, A. J. Holomorphic Hartree−Fock theory and configuration interaction. *J. Chem. Theory Comput.* **2014**, *10*, 4795−4800.
(44) Burton, H. G.; Thom, A. J. Holomorphic Hartree−Fock theory: an inherently multireference approach. *J. Chem. Theor. Comput.* **2016**, *12*, 167−173.
(45) Levine, B. G.; Durden, A. S.; Esch, M. P.; Liang, F.; Shu, Y. CAS without SCF—Why to use CASCI and where to get the orbitals. *J. Chem. Phys.* **2021**, *154*, 090902.
(46) Head-Gordon, M. Characterizing unpaired electrons from the one-particle density matrix. *Chem. Phys. Lett.* **2003**, *372*, 508−511.

https://doi.org/10.1021/acs.jctc.2c00740
J. Chem. Theory Comput. XXXX, XXX, XXX−XXX